University College of Southeast Norway
Faculty of Technology, Natural Sciences and Maritime Sciences

Doctoral dissertation No. 18
2017

Grunde Waag

Air-coupled Ultrasound for Plate Thickness Measurements

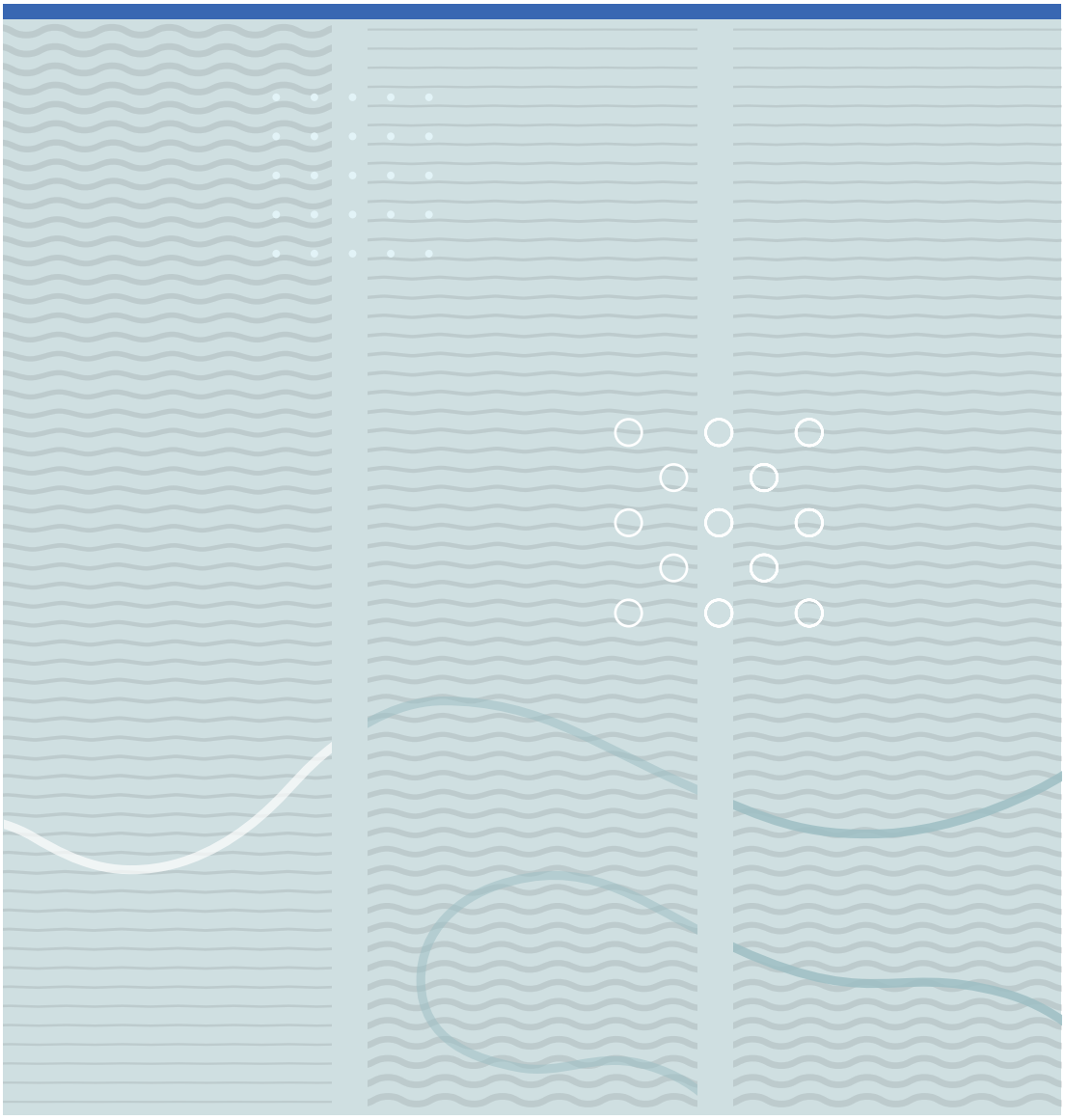

HSN

Grunde Waag

Air-coupled Ultrasound for Plate Thickness Measurements

A PhD dissertation in
Applied Micro- and Nanosystems

Faculty of Technology, Natural Sciences and Maritime Sciences
University College of Southeast Norway
Kongsberg, 2017

Doctoral dissertations at the University College of Southeast Norway no. 18

ISSN: 2464-2770 (print)
ISSN: 2464-2483 (electronic)
ISBN: 978-82-7860-298-0 (print)
ISBN: 978-82-7860-299-7(electronic)

Print: **University College of Southeast Norway**

Preface

This doctoral thesis is submitted in partial fulfillment of the requirements for the degree of Philosophiae Doctor at the Faculty of Technology and Maritime Science, University College of Southeast Norway (HSN), Norway.

The PhD work was carried out at the Department of Maritime Technology and Innovation, Faculty of Technology and Maritime Science, University College of Southeast Norway (HSN), Norway under the supervision of Professor Lars Hoff, HSN, Associate Professor Karina Bakkeløkken Hjelmervik, HSN, Dr. Thor-Andreas Tangen, Halfwave AS, Dr. Petter Norli, Halfwave AS, and Associate Professor Lars Christian Iversen (HSN).

Acknowledgements

First of all, I would like to thank my main supervisor Prof. Lars Hoff for his guidance, feedback and encouragement during this project. I also want to thank my co-supervisors, Petter Norli, Karina Bakkeløkken Hjelmervik, Thor Andreas Tangen, and Lars Christian Iversen for their support and discussions along the way.

I am very grateful for the financial support provided by Halfwave AS, . I was delighted to have the chance to work in the pleasant working environment at the Halfwave office.

Finally, I want to thank my wife, Carina, for always backing me up.

Abstract

Non-destructive testing using ultrasound is well established as a technique of inspecting miscellaneous structures and components. Ultrasonic waves propagating in an elastic solid are sensitive to both the material and geometrical properties of the solid. Decades of experience have shown that it is possible to extract these properties from the waves in an efficient and reliable way in a variety of practical measurement settings. Different techniques have been developed over many decades, and ultrasonic devices are now standard tools for conducting inspection in the oil and gas industry, infrastructure, aerospace industry, and many other fields.

One technique used to examine the properties of a material is based on the acoustic resonance in solid plates. When waves propagate in a plate with finite thickness, they are reflected multiple times within the plate. At some frequencies, this will create a resonance. The resonance frequencies depend, among other parameters, on the thickness of the plate, hence, measurements of the resonance frequencies is a means of determining the plate thickness.

Most ultrasound inspection techniques depend on a liquid coupling between the ultrasound transducers and the solid.

This thesis aims to assess the feasibility of using air-coupled ultrasound for thickness measurements of steel plates, by finding the thickness resonances in the plate. To achieve this, theoretical models for the wave propagation in the plate were developed, featuring the relation between resonances found in a real experimental situation, and the thickness and material parameters of the plate.

The main contributions are:

1. Experimental verification of through-transmission acoustic measurements on a steel plate in air, showing that it was possible to detect several plate resonances. These resonances were used to estimate the plate thickness, demonstrating that it was possible to distinguish between plate segments differing in thickness by 2%.

2. Implementation of a theoretical model to elaborate on the observations of the steel plate measurements. The model is based on the angular spectrum method, includ-

ing the effects of the finite apertures of the transducers; wave propagation in air and elastic waves in the solid plate. The interaction between the plate and the air is handled by plane wave reflection and transmission coefficients. The transducers are described by a plane piston-model.

3. A feasibility study of using a receiver displaced laterally away from the acoustical axis of the transmitter. The scope of the theoretical model was adjusted to include this situation, and then tested experimentally in a through-transmission study on a steel plate in water. The theoretical model was then used to investigate the possibility of conducting pulse-echo measurements on a steel plate in air, using a receiver displaced laterally off the transmitter's acoustical axis. The purpose of this study was to avoid saturating the receiver from the strong first reflection from the air-steel interface, and detect the echoes from reverberations inside the plate.
4. A systematic, theoretical study of the position of the first resonance peak in the received spectra in the through-transmission setup described above. For certain parameter combinations, the first compressional resonance was found to be as low as 0.89 times the plate cut-off frequency, i.e. the simple plane wave assumption can result in errors of up to 11 % compared with the cut-off frequency of the S_1-mode when estimating the plate resonance. A particular focus was on how the down-shift of this resonance depends on the angular spread of the sound field, and how it varies between different material types, especially as a function of the Poisson's ratio of the material.

Contents

Chapter 1

Introduction

1.1 Background and motivation

Non-destructive testing (NDT) is defined in Raj (2002) [1] as 'techniques that are based on the application of physical principles employed for the purpose of determining the characteristics of materials or components or systems and for detecting and assessing the inhomogeneities and harmful defects without impairing the usefulness of such materials or components or system.'

NDT enables in situ inspection of devices, and can provide a rapid and easy method for early detection of failures, e.g. from fractures, cracks or corrosion, and thereby contribute to increased safety and reliability. NDT is a billion dollar industry, with its largest markets in North America and Europe. One important driver of these markets is government safety regulations. Rapid development of infrastructure in emerging markets is also becoming an important driver. In 2002, it was estimated that the cost of corrosion in America amounted to 2 % of GDP [2]. Hence, efficient and reliable NDT methods are valuable tools for both safety and economical reasons.

Several available NDT methods available today are based on different physical principles [3]. The aim of this study is not to give a full overview of the different methods, but discuss some of the useful techniques.

Visual inspection [4] with the eye is perhaps the most basic and widely used inspection technique. Visual inspection can also be performed with a light sensitive sensor such as a camera [4]. Liquid Penetrant Testing (LPT) [5] and Magnetic Particle Testing (MPT) [6] are techniques that uses a second material to enhance the contrast and detectability of a crack or flaw. LPT uses a liquid that penetrates cracks and flaws while MPT magnetizes the target and sprinkle magnetic particles over the target surface to visualize the magnetic field lines that alter if a crack is present. Visual inspection, LPT and MPT require

illumination and a clean surface to be effective.

Visual inspection is effective for detecting cracks and flaws only on the surface of a specimen. This limitation can be overcome with Radiographic Testing (RT) [7] which uses electromagnetic waves in the spectrum beyond that of visible light, for instance, X-rays or gamma rays, that penetrate the target structure. Computed Tomography (CT) is a radiographic technique where a 2D or 3D image can be generated of a non-opaque object. Radiographic Testing techniques requires the source and the detector to be placed on either side of the target object. CT is a lab technique that requires the target to fit the measurement setup. The use of ionizing radiation and radioactive sources is one drawback of the RT techniques since it involves potential health and safety hazards.

In many practical situations, the structures that need to be inspected are large or inaccessible from both sides at the same time, which is required by some RT techniques. This is typical when inspecting large structures and installations such as roads, railways and pipelines. A more flexible solution regarding the size of the target is Magnetic Flux Leakage (MFL) [8]. MFL only needs access to a single side of the target and is widely used for inspection of pipelines in the oil and gas industry. A magnetic field is generated in the target structure, similar to the physical principle of MPT, but sensors are used to detect the flux leakage. MFL is limited to ferroelectric materials and is sensitive to relative changes in dimensions of the target, cracks, and other variations in the material. MFL is a non-contact method, but in practice the sensors must be placed close to the inspection target and cannot conduct absolute measurement of thickness.

Another much applied NDT technology available today is ultrasound. Ultrasound is used both as a point measurement technique and for inspection of large areas of structures by means of guided waves [9]. Ultrasound is used in a variety of settings, from laboratory measurements to the hand held inspection devices deployed by workers in the field. The propagating ultrasound waves are sensitive to both the intrinsic and geometric properties of the propagation medium, and can be used to get information about both types of properties. Examples of the intrinsic properties are: elastic constants, stress levels, and propagation speed and attenuation of elastic waves. Measurements of geometric properties can be thickness, defects, cracks and surface roughness. A review of NDT applications with an extensive list of references can be found in Su and Ye [10].

Ultrasound as an NDT method has important applications in many sectors. Inspection of oil and gas pipelines, power plants, railways and aircraft are applications where ultrasound has become a standard tool. A more comprehensive review of the existing methods can be found in the book by Rose [11].

1.2 Air-coupled ultrasound

The applications of ultrasound for NDT fall into two groups: Applications where the transducers are clamped directly to the target, and those where there is some form of coupling medium between the transducer and the target material. The coupling medium is usually a fluid or a gel. In many practical situations, the use of a couplant is a limitation and clamping the transducer to the target may be impracticable. The couplant may cause an increase in the time spent on inspection, because it needs to be applied for each measurement and perhaps cleaned off afterwards. Further, the couplant might damage or otherwise influence the target, or the size of the structure might make it difficult or impossible to apply. Hence, avoiding application of a liquid couplant can have several benefits. Since most in situ inspections are performed in air, using the air as couplant can have many beneficial properties: Air is readily available and it deforms to the target of interest. However, the strong acoustic mismatch between air and most solids limits the use of air-coupled ultrasound. A review of the existing methods and challenges of air-coupled ultrasound was compiled by Chimenti [12], a few of the main points are repeated below.

The main challenge with air is its low speed of sound and low characteristic acoustic impedance, 342 m/s and 425 Rayl, compared with the properties of the substances to be examined. Liquid couplants have much higher speed of sound and characteristic impedance e.g. water, 1500 m/s and 1.5 MRayl. The low impedance of air compared with most solids, limits the amount of acoustic energy that can be transmitted into the solids. The characteristic acoustic impedance of a piezoelectric element is typically more than ten thousand times higher than air. This impedance mismatch makes it difficult to obtain an effective energy transfer from piezoelectric elements to air, e.g. by matching layers, and gives high losses at both transmission and reception, limited bandwidth and limited dynamic range. The use of membrane transducers can mitigate some of this. Other technologies than the piezoelectric element are also used for generating acoustic waves in air, such as laser based methods or electromagnetic acoustic transducers. For details, cf. the reviews by Remillieux [13] or Green [14].

Even more important than the challenges on creating an efficient broadband air-coupled ultrasound transducer, is the strong acoustic mismatch between the air and most solid targets of interest. The ratio between the characteristic acoustic impedance in air and the solid target determines the amount of energy transmitted into, and out of, the target material, cf. Figure 1. The figure compares the plane wave intensity transmission coefficient at normal incidence for steel embedded in four different coupling media: Water, natural gas at 150 bar and at 50 bar, and air at atmospheric pressure. The values for pressurized natural gas are included to illustrate the gradual transition from a liquid to a

gas at atmospheric pressure. As seen in the figure, a water-steel interface causes a loss at the interface of 20 dB. This is a strong loss, but normally possible to handle. In contrast, the loss through the air-steel interface is about 80 dB, creating large challenges for the transducer and electronics to detect these weak signals.

The low speed of sound in air poses another challenge: a low critical angle. The critical angle for compressional waves in the solid is given by Snell's law as $\theta_{cp} = \sin^{-1} c_f/c_p$, where c_f is the speed of sound in the fluid coupling medium and c_p is the compressional wave velocity in the solid. For shear waves in the solid, the critical angle is $\theta_{cs} = \sin^{-1} c_f/c_s$, where c_s is the shear wave velocity in the solid. The critical angle of the air-steel interface for the compressional wave is around 3°, while the water-steel interface has a critical angle around 15°, see Figure 2. The low critical angle in air makes the alignment of measurement setups important. Acoustical transducers have a finite aperture size, causing an angular spread in the emitted waves. Accordingly, care must be taken in designing a setup to avoid transmitting energy at angles above the critical angle of the target. The use of arrays or geometrically focused transducers can mitigate some of these limitations.

The low speed of sound in air also has consequences for modelling and simulations. A low speed of sound implies short wavelength, i.e. the wavelength in air is much smaller than the wavelength in the solid material. This creates challenges in FEM-simulations of the system, since there must typically be several elements per wavelength to avoid numerical artifacts in a finite element simulation. This leads to large models, which are cumbersome or impossible to handle in many situations. Hence, models for air-coupled ultrasound typically need a combination of different models to handle both the wave propagation in the air and in the solid.

A variety of materials has been studied using air coupled ultrasound, with a range of transduction methods and experimental setups, and described by a variety of theoretical models. Some examples of materials studied by air-coupled ultrasound include plant leaves [15], wood products [16], Plexiglass [17], drug tablets [18], stacked cylindrical spaghetti rods [19], textile materials [20, 21], composite laminates [22], fibre reinforced plastics [23], polymers [23, 24, 25], paper [26, 27], food products [28, 29], and aluminium [30, 31]. Most of the materials listed here can be described as soft, having much lower characteristic acoustic impedance than steel. Hence, the transmission loss at the interface is considerably less than for an air-steel interface.

However, some work has also been done using air-coupled ultrasound on steel. Previous work on steel consists of imaging of spot-welds [32] and excitation of the lowest order antisymmetric mode for imaging of defects [33]. Further applications of air-coupled ultrasound can be found in the review by Chimenti [12]. To my knowledge, through-transmission thickness measurements have not been reported on steel plates.

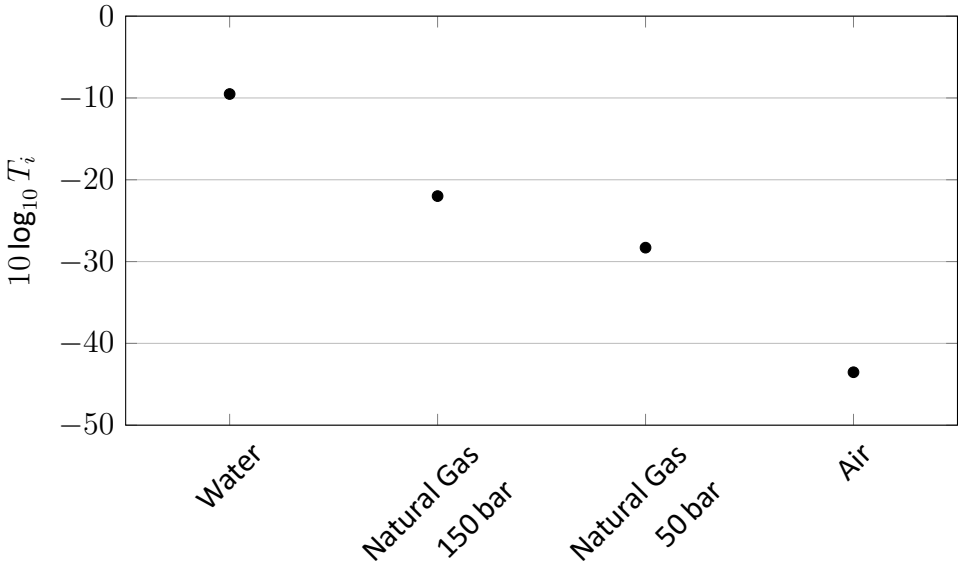

Figure 1: Loss in acoustic intensity from propagation from different materials into a steel plate, described by the transmission from fluid to solid for a plane wave at normal incidence. T_i is the intensity transmission coefficient.

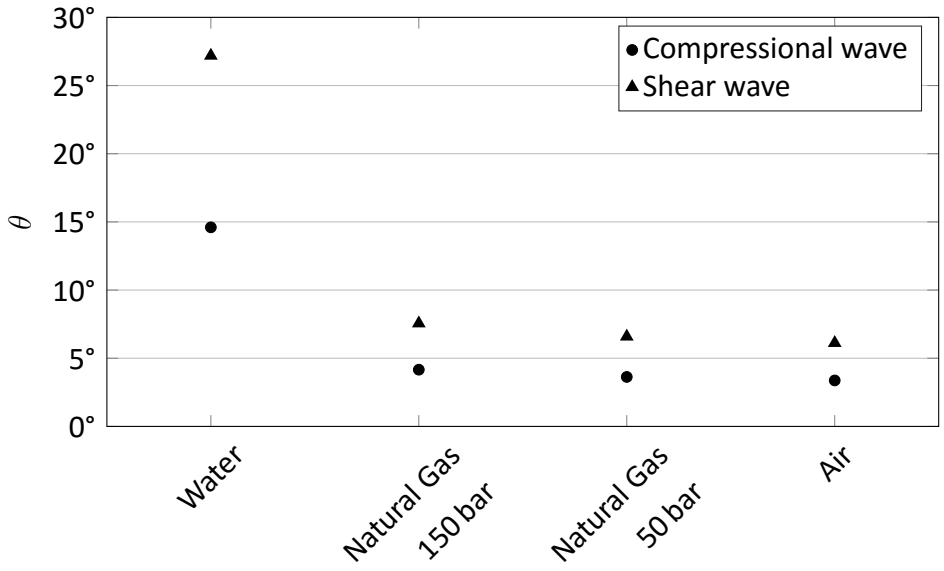

Figure 2: Critical angle for compressional waves $\theta_{cp} = \sin^{-1} c_f/c_p$ (circles), and shear wave $\theta_{cs} = \sin^{-1} c_f/c_s$ (triangles), refracted at a interface between different fluids and steel. c_f is the speed of sound in the fluid, and c_p, and c_s are the compressional and shear wave velocities in steel, respectively.

In addition to being used on a wide variety of materials, air-coupled ultrasound has also been used for miscellaneous applications, such as imaging, defect detection [30], and disbonding detection in multilayer materials [31]. The transmitting and receiving of the ultrasonic waves have also been done using a variety of transduction methods, e.g. electrostatic transducers [17, 34], piezoelectric transducers [15, 35], electromagnetic transducers (EMAT) [36, 14], and pulsed laser [14]. EMAT and laser based methods are strictly speaking not air-coupled ultrasound, as no sound waves are transmitted through the air into the solid. In these examples, the waves generated in the target are converted to ultrasonic waves in the surrounding air, and are picked up by air-coupled acoustical transducers used as receivers.

Theoretical and simulation studies of wave propagation in air-coupled ultrasound have also been reported using several different methods. The finite element method (FEM) modeling is popular [30]. However, the wave speeds in the materials may differ widely, creating challenges for straightforward FEM modelling. The need for many elements per wavelength, combined with the short wavelengths in air limits the distances that can be studied in air using FEM. Furthermore, damping layers or perfectly matched layers are needed to avoid unwanted reflections from the boundaries of the simulation grid. To mitigate this, some authors have chosen to combine FEM models in the elastic solids with analytical wave propagation models in the air [37].

When reviewing the literature, it was found that most experimental systems in air-coupled ultrasound use the through-transmission setup. The main reason for this seems to be that through-transmission avoids the large reflection from the target surface in single-sided measurements. However, a through-transmission setup requires access to the target from both sides, using two aligned transducers. In many practical situations, access from both sides is not possible, e.g. inspection of a ship hull or an oil or gas pipeline. In other cases, alignment and positioning of two transducers is impractical and cumbersome. Hence, single-sided measurements, e.g. pulse-echo, are more practical in many cases, but this implies further requirements on transducers, electronics and signal processing. Air-coupled pulse-echo inspection of solids is not widespread today, but the popularity of such a method might increase if the performance of the transducers improves and new measurement arrangements and signal processing methods become available.

1.3 Elastic waves in plates

The wave propagation of elastic waves in a plate with free surfaces is known as Lamb waves [38]. A plate with a thickness of $d = 2h$ in the z-direction and infinite in the xy-

plane is considered. The geometry is illustrated in Figure 3. Shear and compressional waves propagate in the z-direction, and the surfaces are free, i.e. zero stress at $z = \pm h$. The shear and compressional waves propagate independently with speeds c_s and c_p, respectively. The shear and compressional waves are coupled at the two surfaces of the plate by the zero stress boundary condition. Hence, each reflection of either the shear or the compressional wave creates both a shear and a compressional wave, known as mode conversion. The dispersion relation for the Lamb waves can be found in several textbooks, see for instance Rose [11], and can be expressed as

$$\frac{\tan(qh)}{\tan(ph)} = -\frac{4k_x^2pq}{(q^2-k_x^2)^2}, \tag{1}$$

$$\frac{\tan(qh)}{\tan(ph)} = -\frac{(q^2-k_x^2)^2}{4k_x^2pq}, \tag{2}$$

where k_x is the horizontal wavenumber, $p^2 = \omega^2/c_p^2 - k_x^2$ and $q^2 = \omega^2/c_s^2 - k_x^2$ are the square longitudinal and shear wavenumbers in the z-direction, respectively, with $\omega = 2\pi f$ being the angular frequency. When $k_x^2 > \omega^2/c_p^2$ the compressional waves becomes exponentially damped in the z-direction, known as evanescent waves. The corresponding wavenumber can be written as, see Eq. (2.34) in [39], $p = i\sqrt{k_x^2 - \omega^2/c_p^2}$, with $i = \sqrt{-1}$. For shear waves the evanescent region exist for $k_x^2 > \omega^2/c_s^2$ and the wavenumber can be written as, see Eq. (2.35) in [39], $q = i\sqrt{k_x^2 - \omega^2/c_s^2}$.

The solutions of Eq. (1) and Eq. (2) are found as a discrete set of modes. The solutions of Eq. (1) and Eq. (2) are referred to as the symmetrical and anti-symmetrical modes, respectively. Figure 4 shows the dispersion curves, i.e. the relation between the horizontal wavenumber k_x and the frequency ω for nine different materials. The antisymmetric modes are solutions of Eq. (2), while the symmetric modes are solutions of Eq. (1). The nine materials are selected as examples having different Poission's ratios, and are the same materials as those covered later in the thesis in *Paper C*. The software used to compute the dispersion curves was provided by Dr. Fabrice Prieur[1], Department of Informatics, University of Oslo. The Lamb wave modes are in this work labeled by the type of wave at the cut-off frequencies, as defined in equations (2)-(5) in Prada et al. [40].

1.3.1 Cut-off frequencies

Letting the horizontal wavenumber approach zero, i.e. $k_x = 0$ in Eq. (1) and Eq. (2), yields the equations for the cut-off frequencies, which in most cases is the lowest frequency at

[1] fabrice@ifi.uio.no

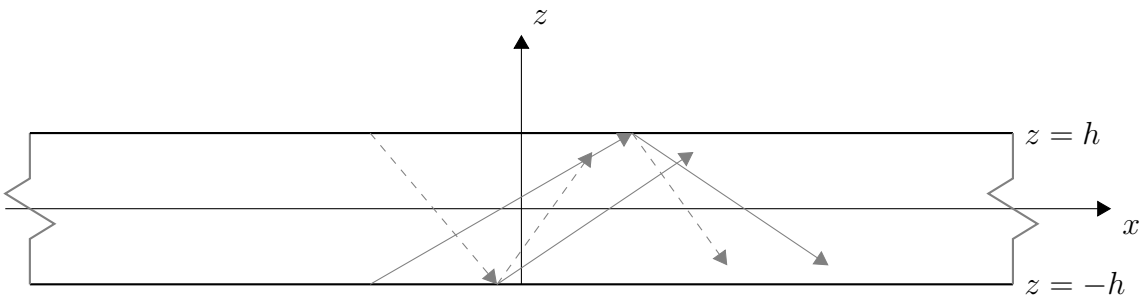

Figure 3: The geometry of a plate with thickness of, $d = 2h$, and infinite in the xy-plane. Shear waves (dashed lines) and compressional waves (solid lines) propagate in the plate and are reflected on the top and bottom plate boundaries. When a compressional or a shear wave is reflected at one of the plate boundaries, it is reflected as both a compressional and shear wave.

which a certain mode can exist [41],

$$qh = \pi\frac{n'}{2} \qquad (n' = 1, 3, 5, ...), \tag{3}$$

$$ph = \pi\frac{n''}{2} \qquad (n'' = 0, 2, 4, ...), \tag{4}$$

for the symmetric case, and [41]

$$ph = \pi\frac{n'}{2} \qquad (n' = 1, 3, 5, ...), \tag{5}$$

$$qh = \pi\frac{n''}{2} \qquad (n'' = 2, 4, 6, ...), \tag{6}$$

for the antisymmetric case. These two equations can be expressed as a function of the shear and compressional speed of sound,

$$f_{np} = n\frac{c_p}{2d} \tag{7}$$

and

$$f_{ns} = n\frac{c_s}{2d}, \tag{8}$$

where $n = 1, 2, 3, ...$ is the order of the mode. Eq. (7) and 8 are also known as the thickness modes, or half wavelength resonances. Note that there are modes which propagate at lower frequencies than the cut-off frequency, hence the term is a misnomer in the case of Lamb waves, but is still widely used. Two examples of modes that exist for frequencies below the cut-off, is the first and second symmetric modes, explored in *Paper C*. Throughout this thesis the symmetric and antisymmetric Lamb modes are labeled according to the integer n in the equations for the cut-off frequencies, Eq. (7) and Eq. (8).

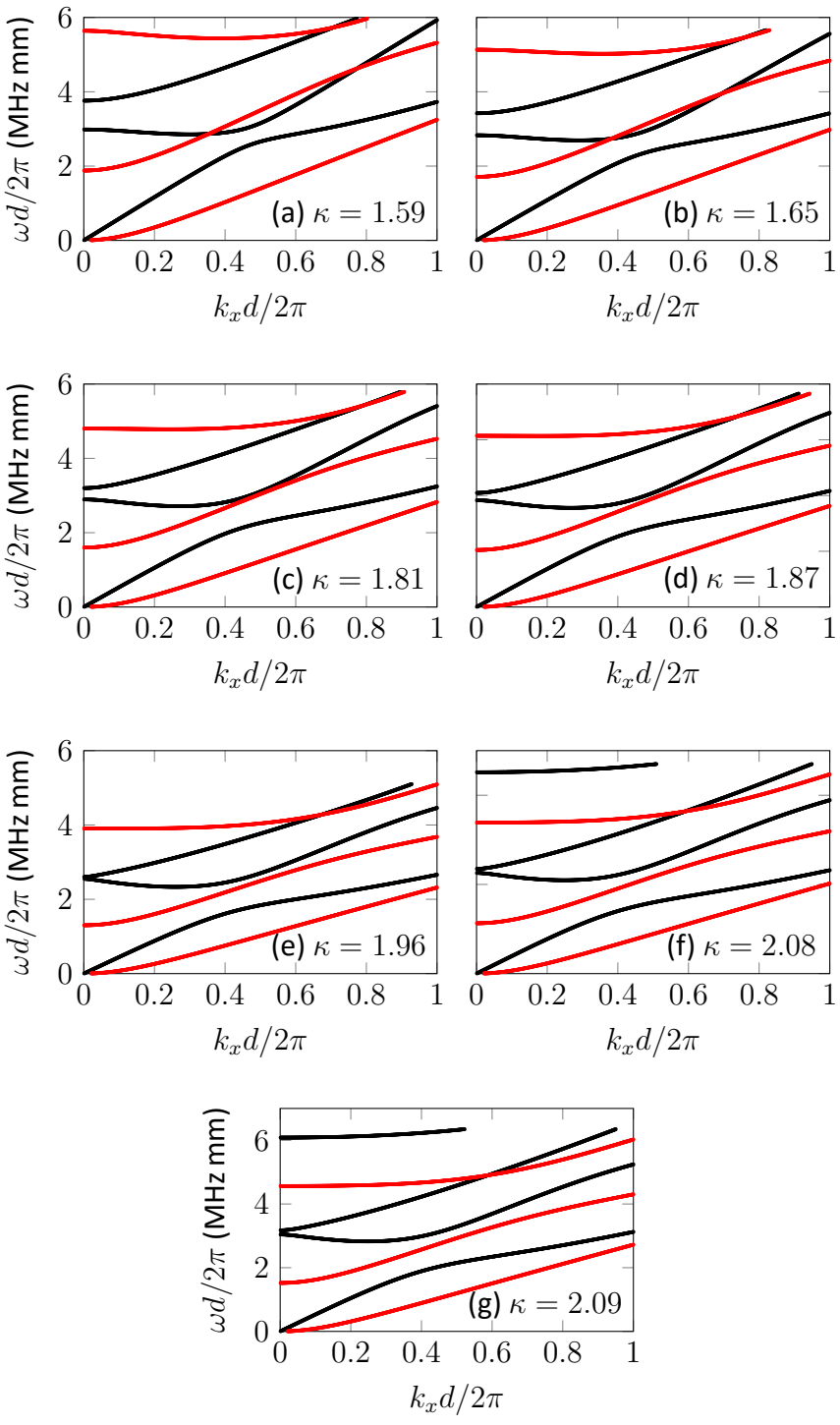

Figure 4: Symmetric (black) and antisymmetric (red) dispersion curves for nine material chosen to span a range of different values of $\kappa = c_p/c_s$, (a) Fused Quartz, (b) Crown glass, (c) Steel, (d) Brass, (e) $BaTiO_3$, (f) Copper and (g) Aluminium. See Table 1, *Paper C* for material properties used in these calculations.

1.3.2 Leaky Lamb modes

In practice the elastic plate is not in vacuum, and there is an interaction between the sound pressure in the fluid and the wave propagation in the elastic plate. In this situation, the waves in the plate are usually referred to as leaky Lamb waves, since some of the energy in the plate leaks out to the surrounding fluid at each reflection. The energy loss from internal reflections is taken into account by the pressure transmission and reflection coefficients for a plane wave with frequency ω and angle of incidence θ, impinging on a plate embedded in a fluid [42],

$$R(\omega,\theta) = \frac{AS - Y^2}{(S+iY)(A-iY)}, \tag{9}$$

$$T(\omega,\theta) = -iY\frac{A+S}{(S+iY)(A-iY)} \tag{10}$$

where

$$Y = \frac{1}{4} y \sin P \sin Q, \tag{11}$$

$$y = \frac{Z_f}{Z_p} = \frac{\rho_f c_f / \cos\theta}{\rho_s c_p / \cos\theta_p}, \tag{12}$$

is the fluid-solid impedance ratio, ρ_f is the fluid density, ρ_s is the density of the solid, $Z_f = \rho_f c_f / \cos\theta$, $Z_p = \rho_s c_p / \cos\theta_p$, θ_p and θ_s are the propagation angles for the compressional and the shear wave in the solid plate, respectively, $P = \omega d \cos\theta_p / c_p$ and $Q = \omega d \cos\theta_s / c_s$.

$$A = \Delta_a \sin\left(\frac{1}{2}P\right) \sin\left(\frac{1}{2}Q\right), \tag{13}$$

and

$$S = \Delta_s \cos\left(\frac{1}{2}P\right) \cos\left(\frac{1}{2}Q\right). \tag{14}$$

Finally Δ_a and Δ_s are the characteristic determinants for the symmetric and antisymmetric modes of the Rayleigh-Lamb equations, Eq. (1) and Eq. (2), defined by,

$$\Delta_s = \cos^2(2\theta_s) \cos\left(\frac{P}{2}\right) \sin\left(\frac{Q}{2}\right) + \left(\frac{c_s}{c_p}\right)^2 \sin(2) \sin(2\theta_s) \sin\left(\frac{P}{2}\right) \cos\left(\frac{Q}{2}\right), \tag{15}$$

$$\Delta_a = \cos^2(2\theta_s) \sin\left(\frac{P}{2}\right) \cos\left(\frac{Q}{2}\right) + \left(\frac{c_s}{c_p}\right)^2 \sin(2\theta_p) \sin(2\theta_s) \cos\left(\frac{P}{2}\right) \sin\left(\frac{Q}{2}\right), \tag{16}$$

Eq. (9) and Eq. (10) are formulated differently from the corresponding equations in *Paper C* and *Paper D*, but are equivalent [42].

Assuming that a pressure wave impinges on the top surface in Figure 3, the reflection coefficient Eq. (9) is the ratio between the freefield pressure of the reflected wave and

the freefield pressure of the incoming wave. The transmission coefficient is the ratio between the freefield pressure amplitude on the bottom side of the plate and the freefield pressure amplitude on the top side. The multiple reflections inside the plate and the loss at the fluid-solid interfaces are included in the model. Absorption due to the wave propagation within the solid can be included by a complex speed of sound or wave number. The transmission coefficient for a steel plate embedded in air is shown in Figure 5, where the color scale has been adjusted to enhance the areas where transmission occurs.

The zeros of the reflection coefficient, Eq. (9), correspond to maxima in the transmission coefficient, where $|T| = 1$. If the characteristic impedance of the fluid is small compared with that of the solid, these are close to solutions of the Rayleigh-Lamb equations, Eq. (1) and Eq. (2). However, deviations are expected when the impedance of the fluid approaches that of the solid [43]. Figure 6 and Figure 7 show the plane wave pressure transmission coefficients from a fluid-solid interface and a solid-fluid interface respectively. The fluid-solid pressure transmission coefficient involves mode conversion, i.e. that the longitudinal wave in the fluid is transmitted into a pressure and a shear wave in the solid. For the solid-fluid interface the shear wave is converted into a pressure wave. The material parameters used for the computations in Figure 6 and Figure 7 are $c_p = 5950\,\mathrm{m/s}$, $c_s = 3230\,\mathrm{m/s}$, $\rho_s = 7950\,\mathrm{kg/m^3}$, $c_f = 340\,\mathrm{m/s}$ and $\rho_f = 1.2\,\mathrm{m/s}$.

The plane wave reflection and transmission coefficients, Eq. (9) and Eq. (10), are implemented in Matlab (The MathWorks, Natick, MA, USA), as detailed in *Paper D*. This implementation is the basis for most of the theoretical calculations used to study the various phenomena investigated in this thesis.

The convention used for the time dependence in Eq. (9) and Eq. (10) is $\exp\{i\omega t\}$ [42]. This convention has been used throughout this thesis, except for *Paper A*, where the convention $\exp\{-i\omega t\}$ was used.

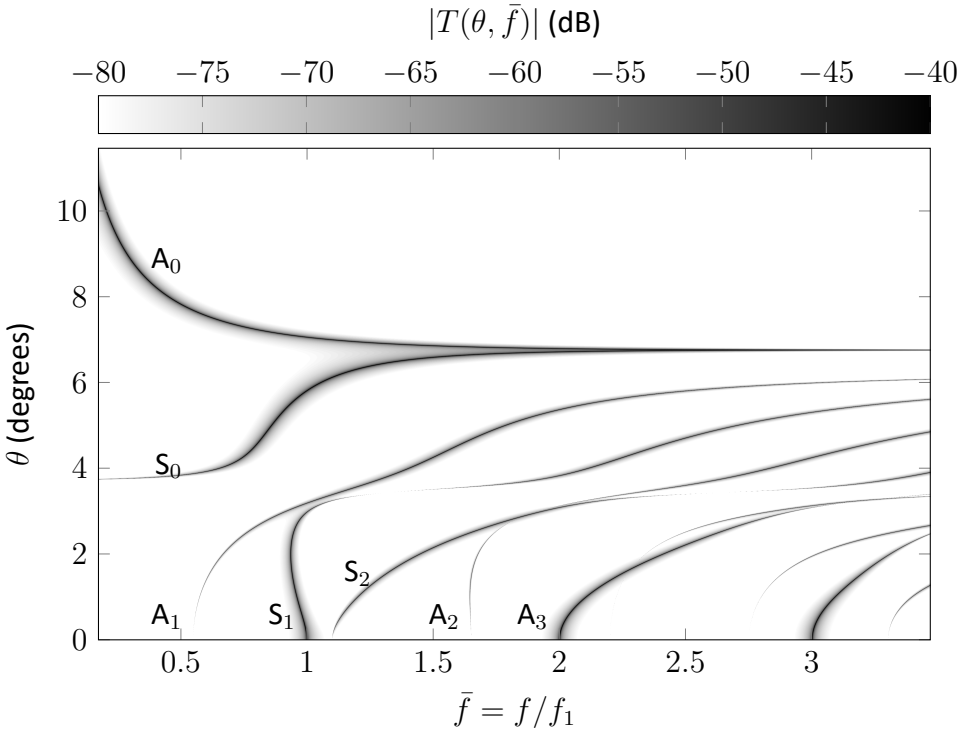

Figure 5: Transmission coefficient for a steel plate embedded in air, where some of the modes have been labeled. The frequency is normalized to the value of the first compressional wave resonance at normal incidence, $f_1 = c_p/2d$, i.e. the cut-off frequency of S_1.

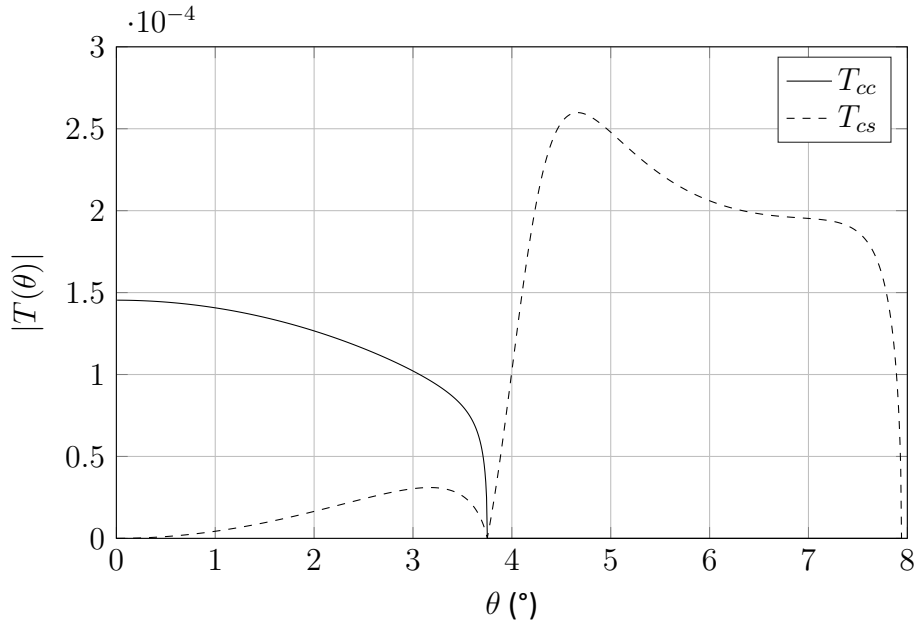

Figure 6: Pressure transmission coefficients from a compressional wave in the fluid to a compressional wave in the solid T_{cc} and to a shear wave in the solid T_{cs}.

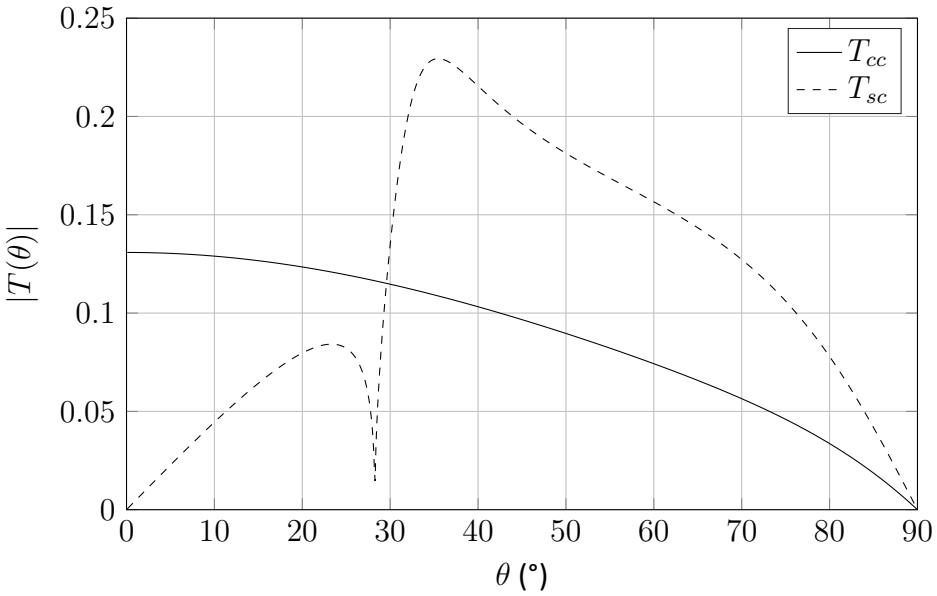

Figure 7: Pressure transmission coefficients from a compressional wave T_{cc} and a shear wave T_{sc} in the solid, to a compressional wave in the fluid halfspace.

1.4 Zero group velocity modes

Some Lamb modes have been shown to have zero group velocity for non-zero wavenumbers [44]. When the Lamb mode group velocity vanishes for non-zero wavenumbers it is referred to as zero group velocity (ZGV) modes. ZGV modes have been identified to exist for symmetrical and antisymmetric modes up to orders 10 and 9, respectively, and for a wide range of Poisson's ratios [40]. One of the modes with an observed ZGV-point is the first symmetrical mode, referred to as S_1-ZGV. Figure 8 shows the dispersion curves for the S_1 and S_2 modes for steel and is a zoom in of Figure 4c. The cut-off frequency for the S_1 mode ω_c, i.e. the frequency at $k_x = 0$, has been labeled. For wavenumbers below the ZGV point, the slope is negative, which means that the group velocity is negative and has the opposite sign of the phase velocity. It is referred to as a backward propagating wave and is referred to as the S_{2b}-mode. For the S_1-mode the group velocity is positive.

Among the phenomena reported for the S_1-ZGV mode are

- strong resonance [40, 45],
- power law decay [46, 47]
- efficient transmission through a 5.46 mm Lucite plate and a 8.1 mm thick graphite–epoxy composite plate in air at frequencies corresponding to k_0 [48], i.e. 223 kHz and 183 kHz respectively.

The physical explanation for the ZGV modes is still a subject of debate [49], and is not a topic of this study.

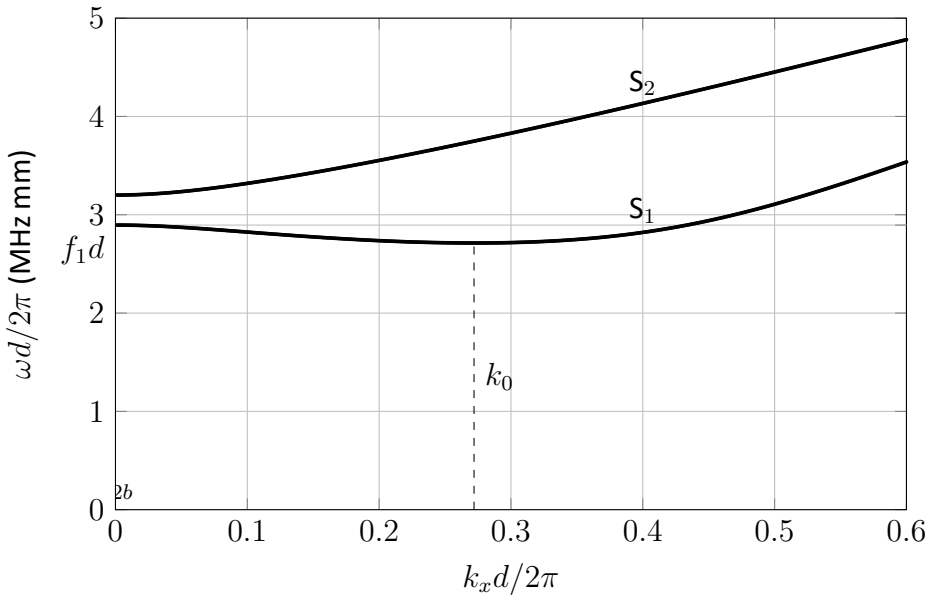

Figure 8: The S_1 and S_2 modes for steel plate with free surfaces and $c_p = 5790\,\mathrm{m/s}$ and $c_s = 3200\,\mathrm{m/s}$. The S_1-ZGV point at k_0 is marked with a dashed line, and the cut-off frequency ω_c is marked on the y-axis.

A group of non-contact techniques that produce and senses ultrasound in metals and other materials, is the laser-based techniques [50]. The laser based methods have been successful in studying Lamb waves in plates [51, 52] and more specifically, the ZGV modes [40]. When generating ultrasonic waves, a small spot on the material surface is heated using laser pulses. Consequently, thermal expansion generates a wave propagating in the material. For detection of ultrasound, a laser interferometer has been used. The interferometer can measure displacement at the surface of a material, a wave propagating through a medium or a wave propagating through a transparent solid [52, 53]. These techniques have also been combined with other methods of generation and reception of ultrasound.

Mattei and Adler [51] used laser interferometry in combination with a contact transducer to generate and measure the propagation speed of Rayleigh and Lamb waves in solids. Clorennec et al. [54] excited the minimum frequencies of the S_1 and A_2 modes and used the ratio between those two frequencies to determine the compressional and shear velocities and solids. Prada et al. [40] investigated the ZGV mode and the backward propagating wave both experimentally and theoretically. The temporal behavior of ZGV resonances was studied in [46, 47], where a power law and an exponential decay in time of the ZGV resonances were observed. In Prada et al. [46] the exponential decay of the S_1-ZGV mode was used to measure material damping.

The Impact Echo method has been established as an important technique in civil engineering for inspecting concrete and masonry structures [55]. The impact echo method

uses the transient response of a point mechanical impact on the target. The resonance frequency of the target is measured, and is then used to determine either the thickness or the speed of sound of the target. In the simplest case, when the compressional speed of sound is known, the thickness can be found by using the equation Eq. (7) with $n = 1$. The underlying assumption of Eq. (7) is that the impact creates a compressional wave, which is reflected back and forth within the target, creating a resonance described by Eq. (7). Deviations from Eq. (7) are taken into account by an empirical correction factor β, with a value of less than one. A theoretical basis for the correction factor is provided by Gibson et al. [56], linking the observed resonance frequency to the ZGV mode of the S_1 Lamb mode. This study describes how the correction factor β depends on the Poisson's ratio, using concrete with Poisson's ratios varying from 0.16 to 0.25 Conventional Impact Echo testing is done with a receiving sensor mounted in contact with the target, while Tsai and Zhu [57] investigated the use of a contactless receiver sensor to obtain the resonance frequency of the target. They used a steel ball to create the impact and a microphone to measure the generated sound waves. The signals measured by the microphone consist of a wave coming directly from the impact between the steel ball and the concrete target, a leaky surface wave, and the vibrations of the target. A time window is used to filter out the direct wave and the leaky surface wave from the time signal before the spectrum is computed. Both the S_1-ZGV and the A_2-ZGV are observed in numerical finite element simulations and laboratory measurements.

1.5 Bounded beam interaction with plates

The plane wave reflection and transmission coefficients Eq. (9) and Eq. (10) describe how plane waves at a certain frequency and angle of incidence are reflected or transmitted through a solid plate. However, for many experimental situations, the plane wave assumption is not sufficient, and the effect of finite apertures or bounded beams needs to be included. The chosen model for this work is the Angular Spectrum Method (ASM) mainly based on Orofino and Pedersen [58]. A more detailed discussion can, for instance, be found in the theory of Forier Acoustics [59]. The ASM uses the 2D Fourier transform to transform a field $u(\vec{x})$, e.g. velocity or pressure, observed in a plane perpendicular to the z direction to the wavenumber plane spanned by k_x and k_y. For a wavenumber vector $\vec{k}$, k_x and k_y are the components in the x and y directions respectively. $k_z = \sqrt{k^2 - (k_x^2 + k_y^2)}$ is the wavenumber component in the propagation direction, where k is the length of the wavenumber vector. When $k_x^2 + k_y^2 > k^2$ the wave is decaying exponentially in the propagation direction and is called an evanescent wave. For an evanescent wave propagating in the positive z direction $k_z = -i\sqrt{(k_x^2 + k_y^2) - k^2}$. This is an extension of the Fourier transform to two dimensions.

Assume that the field variable u is known in the xy-plane at $z = 0$, denoted $u_0(x, y)$. Here, u can represent any parameter of the acoustic field, e.g. pressure, velocity or displacement. The 2D spatial Fourier transform of u is defined as,

$$U_0(k_x, k_y) = \iint_{-\infty}^{\infty} u(\omega; z = 0) \exp\{i(k_x x + k_y y)\}\, dxdy. \tag{17}$$

U is often referred to as the angular spectrum of the quantity u, and can be interpreted as a plane wave decomposition of the spatial velocity field $u(x, y)$. The spatial velocity field can be reconstructed from the angular spectrum U by using the inverse 2D Fourier transform,

$$u_0(x, y) = \frac{1}{(2\pi)^2} \iint_{-\infty}^{\infty} U_0(k_x, k_y) \exp\{-i(k_x x + k_y y)\}\, dk_x dk_y. \tag{18}$$

The angular spectrum can be propagated to a new xy-plane at any position z' by multiplying with a complex phase factor,

$$U_{z'}(k_x, k_y) = U_0(k_x, k_y) \exp\{-ik_z z'\} \tag{19}$$

where k_z is the component of the wavenumber in the z-direction. After propagating the angular spectrum to the position z', the spatial field $u_{z'}(x, y)$ can be computed by applying the inverse Fourier transform Eq. (18),

$$u_{z'}(x, y) = \frac{1}{(2\pi)^2} \iint_{-\infty}^{\infty} U_0(k_x, k_y) \exp\{-i(k_x x + k_y y)\} \exp\{-ik_z z'\}\, dk_x dk_y. \tag{20}$$

One of the reasons for the ASM being so attractive, is that the highly computationally efficient Fast Fourier Transform (FFT) can be used to compute the transforms Eq. (17) and Eq. (18).

Reflection from and transmission through a plate can now be handled by using the plane wave reflection and transmission coefficients. The reflection and transmission coefficients for pressure determined earlier, Eq. (9) and Eq. (10). Using this approach, reflection from a plate is handled by multiplying each of the components of the plane wave decomposition $U(k_x, k_y)$ by the plane wave reflection coefficient Eq. (9), at the corresponding angle and frequency. Similarly, transmission through a plate is handled by multiplying $U(k_x, k_y)$ by the plane wave transmission coefficient Eq. (10). If the angular pressure spectrum at the top of a plate $U_t(k_x, k_y)$ is known, the pressure at the bottom of the plate can be written as

$$U_b(k_x, k_y) = U_t(k_x, k_y) T(k_x, k_y), \tag{21}$$

where $T(k_x, k_y)$ is the plane wave transmission coefficient for pressure. Further details about how this is handled and implemented in the software are presented in *Paper D*.

Other methods and techniques used to study interaction of bounded beams with plates exist in the literature. A thorough overview can be found in the work by Aanes [39]. Finite element models (FEM) have for instance been applied to study single-sided pitch-catch experiments in 2D [30]. Full 3D FEM simulations for the transmission through a plate have been done and compared with measurements in a water tank [39]. FEM has also been used in combination with other analytical methods, for instance ASM. The same FEM used by Aanes was also used in combination with ASM [39], where the transmitter is simulated in FEM, while the wave propagation in the water and through the plate is computed using the ASM method. Other authors have tried to avoid the effects of a finite aperture experimentally, by creating systems where the sound field can be approximated by a plane wave. This can either be done by using a large transducer aperture [60], or a setup similar to a synthetic aperture [42].

FEM is more computational intensive than the ASM, where the optimized FFT algorithms or analytical expressions can be used. This is especially true for wave propagation over many wavelengths. In addition, FEM requires detailed knowledge of the transducer in order to improve the accuracy beyond the plane piston model. On the other hand, ASM is limited to geometries where the plane wave reflection or transmission coefficients are known, while FEM can be used for complex 3D structures. In order to avoid the effects of bounded beams, a transducer with a large aperture can be used. However, a large aperture is often inconvenient when taking measurements in the field.

In most practical systems, a finite aperture transducer is used, giving a bounded beam where the angular spread of the sound field will cause significant deviations from the plane wave approximation. One observed effect of a bounded beam, is that the resonance peak from the S_1 mode is shifted down at normal incidence, compared with the cut-off frequency of the mode, given by f_n. Several authors have observed the down-shift effect with a variety of measurement setups [45, 39, 61, 62, 63, 64]. As described earlier, the down-shift is related to the S_1-ZGV mode. Holland and Chimenti [45] found the S_1-ZGV resonance of a plate in air to be 10 dB above other modes for several different materials. They used the favourable transmission properties of the S_1-ZGV mode for through-transmission imaging of Lucite plates in air. Their study concludes that small or focused apertures must be used to excite the resonance at the S_1-ZGV mode, but does not provide numerical values, e.g. for how small aperture or at what frequency the S_1-ZGV mode appears for a given aperture. Aanes et al. [63] reported a down-shift of the first compressional resonance compared with the plane wave model, both at normal incidence and at 1° angle of incidence. An angular spectrum model was used to study deviations from the simple plane-wave theory for Poisson's ratios from 0.01 to 0.49 The study also showed that the beam transmitted through the solid plate close to the S_1-ZGV frequency is narrowed or collimated. Aanes' study provides a set of systematic simulations

on how the resonances shift as the Poisson's ratio of the plate varies. However, the effect of varying transducer apertures and distances to the target was not examined.

1.6 Thickness measurements

The thickness of a solid plate can be measured using ultrasound by miscellaneous methods. The ultrasonic thickness gauge is a readily-available tool used off the shelf as a handheld device. The most common method used in ultrasonic thickness gauges, is by emitting a waveform and measuring the time of arrival of the pulse reflected from the rear of the target plate. The thickness is then found by multiplying the speed of sound in the target by the time of flight. This method requires the multiple echoes from the back wall to be separately identified, requiring a short pulse. Separation of the echoes and accurate determination of the time of flight may prove difficult in the case of thin plates, see the analysis by Demirli and Saniie [65].

The use of guided waves is another and more sophisticated method for estimating the thickness of plates. This can, for instance, be done by measuring the group or phase velocities of various modes in the plate, as described by Etaix [66]. Gao et. al. [67] used laser based ultrasound measurements of the dispersion curves, applying them to a theoretical model in order to infer the thickness. This technique can be used to measure not only thickness, but also the elastic parameters of a plate [68].

Instead of doing the evaluation in the time domain, as done for the pulse-echo time-of-flight method, it can be done in the frequency domain using resonances in the received spectra. In the simplest case, this method uses the thickness resonances of the plate to estimate the thickness. For a plane wave transmitted at normal incidence through an elastic plate, the plane wave reflection coefficient Eq. (9) predicts that acoustic energy is mostly transmitted at the half-wavelength resonance frequencies,

$$f_n = n\frac{c_p}{2d}, \tag{22}$$

where n is the harmonic order and c_p is the compressional wave velocity in the plate. Known as the thickness compressional modes, these resonances can be used to calculate the plate thickness, d, when the wave velocity c_p is known. Eq. (22) is recognized as the cut-off frequencies of the Lamb modes which were found in Eq. (7). Note that in this simplest assumption, plane wave normal incidence, shear waves will not be excited.

Work on thickness measurements of plates in air, using air-coupled acoustic transducers, is limited. Alvarez-Arenas [28, 69] measured simultaneously the velocity and thickness

of polyether sulfone and cellulose membranes and of dry-cured ham using a through-transmission setup. The presented method compares two transmission measurements, evaluated in the frequency range around the first plate resonance, i.e. f_1 in Eq. (22). The first reference measurement is taken without the sample, only the transducers in air. Then, a second measurement is taken with the target inserted. The theory used in this work assumes a plane wave at normal incidence, so no correction is made for the angular spread from the finite aperture of the transducers. McIntyre et. al. [70] used capacitive acoustic transducers to do through-transmission measurements of paper. They used Eq. (22) to estimate the speed of sound c_p from a measurement of f_1 on paper with known thickness, without compensation for frequency shift from finite aperture and ZGV modes. If the compressional velocity c_p is known, this method can be used to estimate the thickness from Eq. (22). Note that correction of Eq. (22) for the down-shift from the ZGV mode, as illustrated in Figure 8, requires a priori knowledge of the material properties of the sample, notably the Poisson's ratio, in addition to the compressional wave velocity. Hence, this correction can be done to estimate thickness for a known material. Correcting for the down-shift when estimating the velocity for a material of known thickness is not so straightforward.

Chapter 2

Research goals and conclusions

2.1 Research goals

Thus Ph.D. aims to examine the potential of using air-coupled ultrasound to measure thickness of steel plates, based on half-wavelength thickness resonances. This shall be evaluated experimentally and by means of theoretical models. The three main research questions addressed in this thesis are summarized as:

- How can the thickness of steel-plates be measured using an acoustic through-transmission technique, with access from both sides of the sample?
- How can a pulse-echo technique be implemented? This requires access from one side of the sample only, but creates a very strong reflection from the air-steel interface.
- How do the resonances observed in a realistic system using transducers with finite apertures and giving a bounded beam, differ from the idealized solutions derived from simple plane wave models?

The experimental setup is shown in Figure 9. The transducer, Tx, transmits an ultrasonic pulse into the air, and this pulse propagates to the solid plate. At the air-plate interface, some of the energy in the pulse is reflected, and some is transmitted into the plate, where it is reflected back and forth within the plate. For each reflection inside the plate, some energy will also be transmitted out into the air. On the front side, this energy will propagate back to the transmitting transducer, Tx, while on the rear side, it will propagate to the receiver, Rx, on the opposite side. The recorded signal from a pulse-echo measurement, where the transmitter and receiver are the same transducer, will consist of an initial reflection from the plate and a long decaying tail originating from internal reflections in the plate. Since the characteristic acoustic impedances of the plate and the air are very different, the first reflection from the air-plate interface is expected to be very

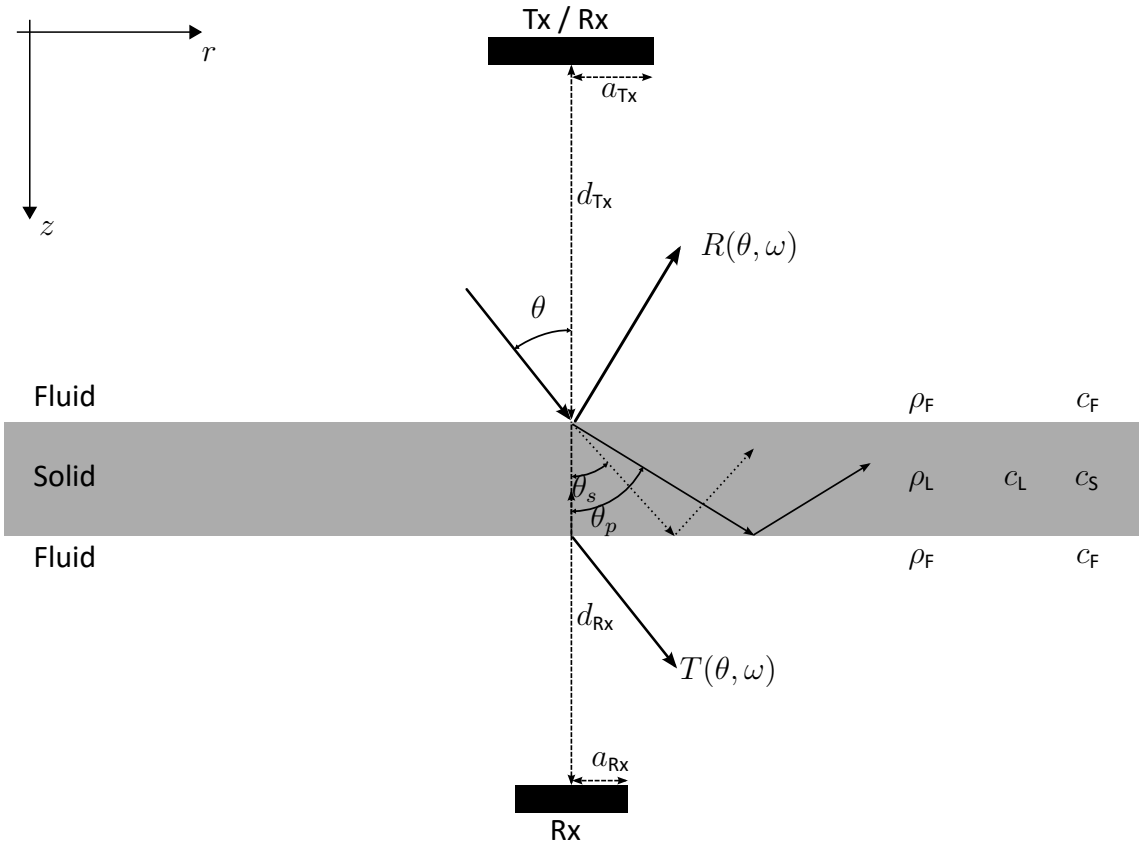

Figure 9: Illustration of the acoustic pulse-echo and through-transmission measurement setups. A single plane wave propagating from the transmitter *Tx* at an angle θin the fluid is illustrated with an arrow. The corresponding refracted compressional and shear waves and the transmitted waves are arrowed. The compressional and shear waves propagate at angles θ_p and θ_t respectively.

strong compared with the following tail. The tail of the signal will contain resonances from the internal reflections within the plate, and from this, information about the thickness of the plate can be extracted. An important task of this project has been to develop a good understanding and theoretical models for this system, especially for the relation between the resonances, the plate thickness and material properties, and the properties of the sound field, and to verify this with experimental data. The ultimate goal of the project was to use this information to develop a hand-held device, capable of takin pulse-echo thickness measurements on steel plates in air, and more generally, to provide knowledge to improve other existing ultrasound characterization technology, such as the *ART Scan in-line inspection tool* described in section 2.3.

Previous studies have shown that through-transmission of aluminium is possible with broadband pulses [34] and that thickness measurements can be taken using resonances in plates [28, 69]. When taking on-line measurements in the field, such as those in in-line pipe inspections detailed in section 2.3, measurements of single resonances lack robustness for automatic algorithms, and a single resonance is also very sensitive to noise.

The first study of this thesis, described in *Paper A* investigated if reliable measurements could be taken on a steel plate in air. A through-transmission method was chosen, as this avoids the problem of the very strong first reflection found in a pulse-echo setup. It should be investigated whether the results could be used to detect absolute thickness changes of less than a millimeter, or relative changes of a few percent. Furthermore, theoretical models should be developed and implemented to explain the experimental results, processed as the received spectra. These models should use state-of-the-art theory, including the various plate modes and the bounded sound wave of a realistic transducer, not being limited to a single plane-wave.

In a pulse-echo setup, the very strong reflection from the air-steel interface may saturate the receiving system, or at least create a ring-down of the receiver that will overshadow the tail signal coming from the reflections inside the plate. Since all information about the plate is contained in the tail of the signal, this very strong first echo is a problem in a practical setup. A method to overcome this issue was studied in *Paper B*. This study considers the possibility of moving the receiver laterally away from the acoustic axis of the transmitter, to see if this will reduce the signal level of the first reflection relative to the tail. Further, it was investigated how measuring at a laterally displaced position will affect the peaks in the received spectra, using measurements in a water tank and the theoretical model implemented previously.

When using half-wavelength resonances to estimate thickness, the first approximation is often to assume a single plane wave. However, the plane wave assumption is in many cases too inaccurate, and a better model is needed for the relation between the reso-

nance frequencies and the thickness. Experience from studies of half-wavelength resonances at DNV GL has shown that the f_1 resonance for realistic transducers is shifted down compared with the plane wave assumption, typically by 6 %. The down-shift is also described in the literature, as mentioned previously. The actual value of the down-shift depends on the specific setup, based on the actual parameters of the measurement system. A more comprehensive study on how the down-shift is related to the various parameters of the measurement setup was wanted, which led to the theoretical study presented in *Paper C*. In *Paper C* established theoretical models are employed to map the down-shift of the first resonance, f_1, as a function of parameters of the measurement setup and of the plate material properties. The study used the angular spectrum method, ASM, to describe the wave propagation in the plate and the surrounding fluid. The study was done using water as a coupling medium, in order to obtain a better signal to noise ratio and enable easier experimental verification of the result than is possible in air, i.e. to test the model without the extra complexity arising when using air as coupling medium. The ultimate goal is to be able to apply the method in air-coupled ultrasound. It was expected that similar results will be found when air is used as a coupling medium, but this has not been tested experimentally in this work. High quality quantitative results in air will most likely require further optimization of the transducer and electronics, which was not feasible to do in this project.

Paper A, *Paper B*, and *Paper C* place emphasis on presenting results relevant to the application, i.e. is using resonances to determine the thickness of plates. The theoretical evaluation in these papers is based on ASM, the Angular Spectrum Method. To obtain the results and conclusions described in these papers, an ASM model was implemented in Matlab software. The derivation of the key equations in the ASM model are detailed in *Paper D*. This paper also describes how the model was implemented in Matlab, written as a documentation of the software. Hence, *Paper D* was not written for publication as a scientific paper, but rather as a documentation of the method, implementation and usage of the software, with the intention of being useful for other persons wishing to apply the model for their specific problems, or as a starting point for applying the ASM model to study a different application.

2.2 Experimental setups

The experimental studies done during this project are described in *Paper A* and *Paper B*. Both of these studies use experimental data from acoustic through-transmission systems.

2.2.1 Through-transmission measurements in air (*Paper A*)

The acoustic measurement setup used to measure transmission through steel plates in air, as described in *Paper A*, is illustrated in Figure 10. Two transducers are mounted on opposite sides of a steel plate, one for transmit and one for receive. A broadband pulse is transmitted from the transducer, propagates through the air and the steel plate, and is received and recorded on the opposite side.

Linear chirps with frequencies rangin from 200 kHz to 800 kHz are generated by the function generator (*NI PXI-5421*, National Instruments, Austin, TX, USA) and amplified by the 100 W power amplifier (*E&I 2100L*, Electronics & Innovation, Rochester, NY, USA), and used to drive the transmitting transducer, *Tx*. The transmitter is a custom built piezoelectric transducer (*GPS-I*, Piezo Composite Transducers Ltd, Aberdeen, UK) with center frequency of 540 kHz and diameter 18 mm. The frequency of the transducers and the chirp was chosen to have sensitivity in a frequency range covering the S_1 to A_3 modes at the three thicknesses of the plate being investigated.

In this setup, the sound pulse propagates 40 mm through the air to the steel plate. Part of the sound energy is then transmitted through the plate, and propagates another 40 mm through the air on the opposite side to the receiver (*NCT500-D6*, The Ultran Group Ltd., State College, PA, USA). The receiver has a center frequency of 500 kHz and diameter of 6 mm. The received signal is amplified with a low-noise amplifier (*Olympus Panametrics 5662*, Olympus NDT Inc., Waltham, MA, USA) with 54 dB gain. The amplified signal is digitized with an analog-to-digital converter, DAQ (*NI-PXI 5922*, National Instruments Inc., Austin, TX, USA) at sample rate 15 MS/s with 16 bit resolution, and stored on a computer hard drive. A transparent Plexiglass box was placed on top of the setup to minimize the convection of the air between the transducers and the steel plate, reducing fluctuations in the propagation time in air.

Before the acoustic measurements, as a reference, the thickness of the steel plate was measured with a caliper to 10.15 ± 0.01 mm. This part of the plate was denoted measurement region A. The compressional speed of sound in the solid plate was measured to $c_\mathrm{p} = 5850 \pm 60$ m/s using an ultrasonic thickness gage (*T-Mike E/P/B StressTel*, Deterco Inc., Houston, TX, USA), with the thickness measured above.

To test the ability to estimate thickness, two rectangular areas of the plate, denoted B and C, were machined down. Region C was measured with the caliper to 9.80 ± 0.01mm. Region B was not accessible with the calliper, and was measured with the ultrasonic thickness gage, using the speed of sound measured in region A as input. The thickness of region B was measured to be 10.0 ± 0.01mm.

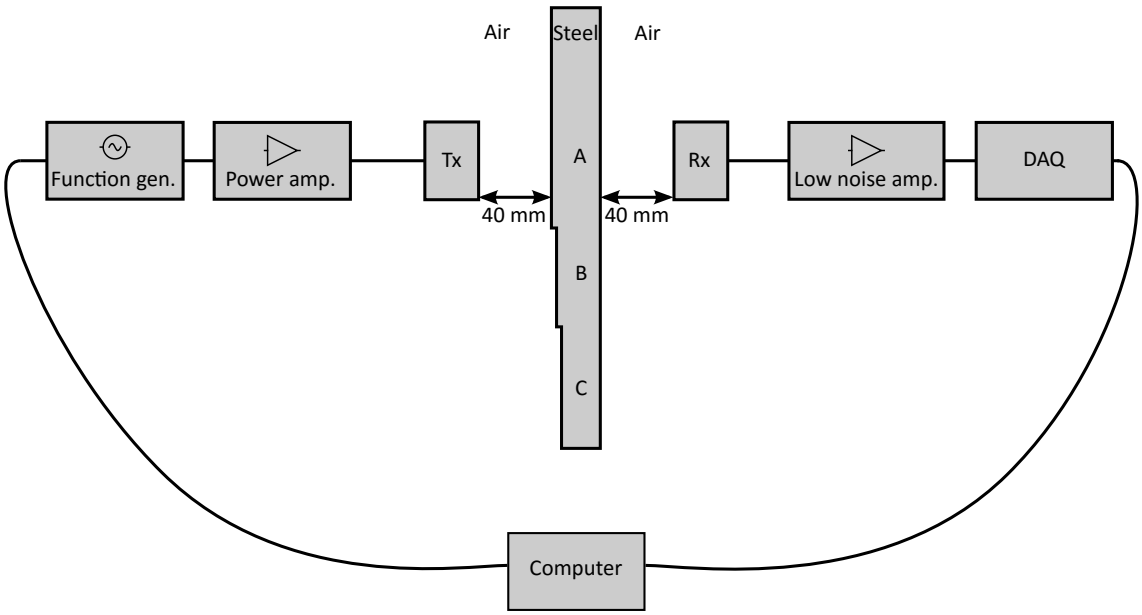

Figure 10: Sketch of the acoustic through-transmission setup used for measurements on a steel plate in air, as described in *Paper A*. Region A is where the steel plate has not been machined, i.e. has the original thickness 10.15 mm. Region B is the part of the plate machined down to 10.00 mm, and Region C where it was machined down to 9.80 mm. The distance from the transducers to the target is 40 mm for both the transmitter *Tx* and the receiver *Rx*.

2.2.2 Measurements using a laterally displaced receiver (*Paper B*)

The effect of using a receiver displaced laterally off the acoustic axis was the topic of *Paper B*. The theoretical predictions in this paper were tested against acoustic through-transmission measurements in a water tank, the setup is shown in Figure 11. Water was chosen instead of air as the coupling medium, in order to obtain higher signal levels in these test measurements. This setup uses the same function generator, power amplifier and transmission transducer as the air-coupled measurements described above.

A sinc pulse with energy in the frequency range from 100 kHz to 2000 kHz is generated by the function generator (NI PXI-5421) and amplified in the power amplifier (E&I 2100L) which drives the transmitter, Tx (GPS-I). The transmitter sends a pulse into the water, and the pulse propagates through the water to the steel plate. The sound transmitted through the steel plate is received by a hydrophone, Rx (PA09054, Precision Acoustics, Dorset, United Kingdom) on the opposite side of the plate. The hydrophone will pick up the pulse transmitted through the steel plate, including reverberations from multiple reflections inside the plate.

The hydrophone is mounted at a fixed distance from the steel plate, but could be moved parallel to the plate, i.e. in a plane normal to the acoustic axis of the transmitter, in order to measure the sound field at varying lateral displacement r. Two scans were done in a

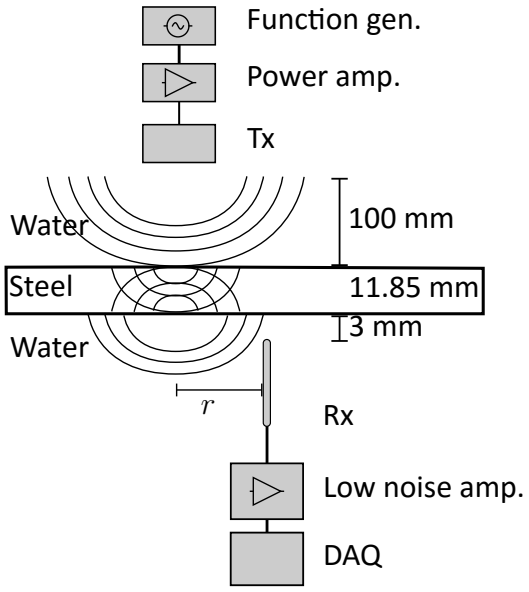

Figure 11: Laboratory setup to measure pulses transmitted through a steel plate at varying lateral displacement, as described in *Paper B*. The measurements were done in a water tank. Transmitted pulses were received with a calibrated hydrophone Rx that could be moved in a plane normal to the acoustic axis of the transmitter.

plane parallel to the steel plate. One scan in the horizontal direction x and one in the vertical direction y, (out of the paper plane in Figure 11). Measurements were taken at displacements r varying from 0 mm to 60 mm, in 1 mm increments.

2.3 Acoustic Resonance Technology

This project was to large extent motivated by a desire to investigate if the ultrasound based ART-technology could be applied using air at ambient pressure as a coupling fluid, and to achieve a consisten theoretical base for the understanding and interpretation of the results obtained in the ART-measurements.

Acoustic Resonance Technology (ART) has been developed by DNV (Det Norske Veritas, now DNV GL) since the 1990s, and was spun out as the company Halfwave AS [71] in 2012. ART is an ultrasound technique for measuring the thickness of plates, mainly steel, based on half-wavelength resonances in the plates. The core of the ART is to transmit a pulse into a fluid and reflect it from a target plate, usually steel, and record the reflected signal. The signal consists of a reflection from the steel surface, followed by a long decaying tail, originating from multiple internal reflections in the plate. These internal reflections cause characteristic resonances in the received spectra, mainly at or close to frequencies corresponding to integer multiples of half wavelengths inside the plate.

The half wavelength resonances can be excited by transmitting an acoustic pulse towards

the plate, and recording the reflected signal. Figure 12 shows a theoretical time signal, typical for an ART measurement on a steel plate embedded in water. The time signal consists of a first reflection, coming from the water-steel interface, followed by a long decaying tail, originating from multiple reflections within the steel plate. The spectra of the first reflection and of the tail are shown in Figure 13. The spectrum of the tail contains peaks at the half wavelength resonances and, in the simplest case, can be predicted by Eq. (7). When the speed of sound in the plate is known, the thickness can be calculated from the frequencies of the peaks in Figure 13. Reflections between the plate and the transducer are also present in a pulse-echo measurement. These can be avoided by time-gating the received signal, and are not included in the model signal in Figure 12. In practice, these plate-transducer reverberations are important because they limit the part of the tail available for frequency analysis. For a transducer-plate measurement setup, the arrival time of the first transducer-plate multiple reflection is twice the arrival time of the first reflection from the plate (see black, solid curve in Figure 12).

The first application of the ART technology was a scanner for inspection of freshwater pipes. This is now operated on license by Breivoll Inspection Technologies AS [72]. The latest application of ART is the in-line gas pipe inspection pig from Halfwave AS, ART scan [71], shown in Figure 14. This scanner is used to inspect gas pipelines from the inside, working in natural gas at 150 bar. The electronics and transducers are mounted on the 'pig', which is pushed through the pipeline by the gas pressure, and the ultrasound unit monitors the wall thickness as it passes along the pipeline.

A key topic of this thesis is to investigate the challenges of measuring the thickness of steel plates or pipes at standard atmospheric pressure. The gas pipeline scanners can be viewed as an intermediate step between the water-coupled scanners and a scanner operating in air at atmospheric pressure. The corresponding challenge in terms of loss due to the impedance mismatch between the coupling fluid and the steel can be seen in Figure 1, and in terms of critical angle in Figure 2.

The work during this project was in part done in collaboration with Halfwave AS. During the project period, I had part-time position at Halfwave AS and used their lab for measurements. This has given me interesting practical applications to work on, and also imposed a few constraints on this work. The equipment used in this work has been limited to what has been available in the lab at Halfwave. Equipment for measuring beam patterns of transducers in air was not available, although such measurements would have given useful information for the studies, especially by providing a more accurate angular spectrum of the sound field, and not having to rely solely on a plane-piston model.

Part of this work has been to acquire a better understanding of the ART method, its possibilities, limitations and how to interpret the signals. The ART method uses resonances

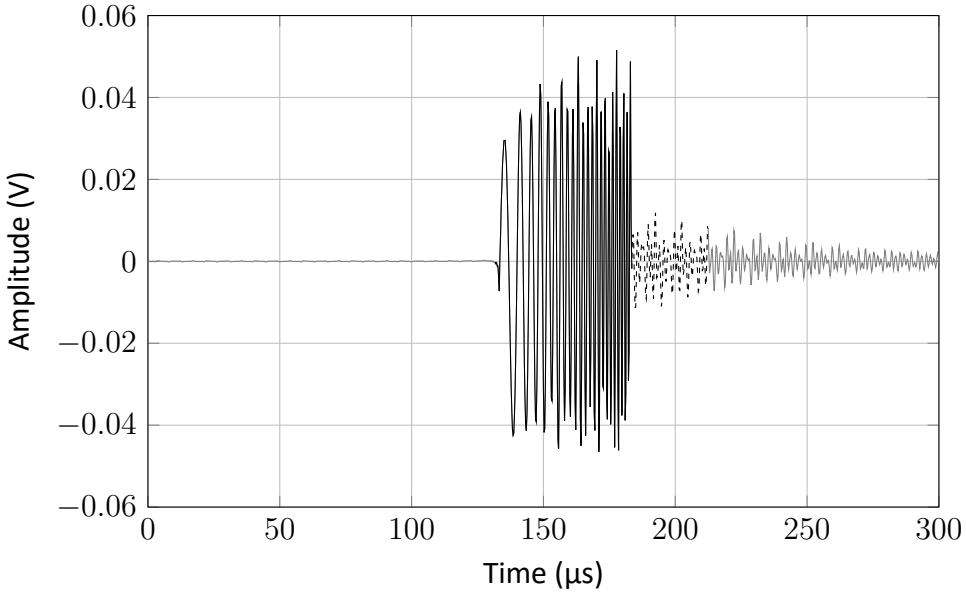

Figure 12: Typical time signal from an ART measurement of a plate with thickness $d = 29.7$ mm and source/receiver plate distance $d_{\mathrm{Tx}} = 100$ mm. The first part of the signal (solid) is identified as the strong reflection from the fluid-steel interface, while the following tail (dashed) is identified as coming from internal reflections in the steel plate. Multiple reflections between the transducer surface and the plate are not included in this simulation, but will limit the maximum length of the tail signal that can be used for thickness evaluation. The first of these reflections should appear at twice the first time of arrival of the signal, in this example around 250 µs.

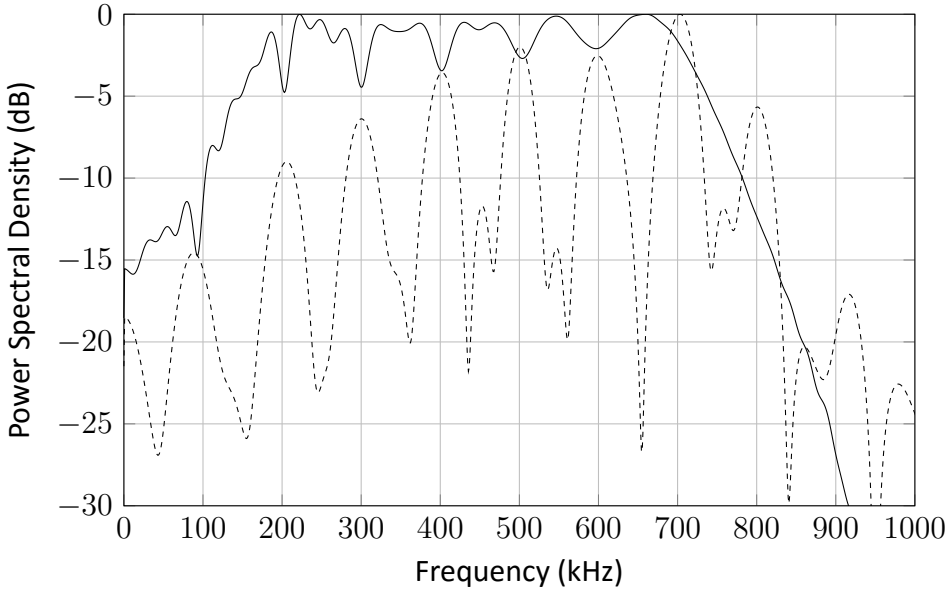

Figure 13: Power spectra of the example ART signal in Figure 12, normalized to the maximum power. The spectra are calculated from the first reflection (solid) and the tail (dashed). Both spectra are normalized to their maximum values. Note the marked resonant structure of the tail signal, and how this is suppressed in the first echo.

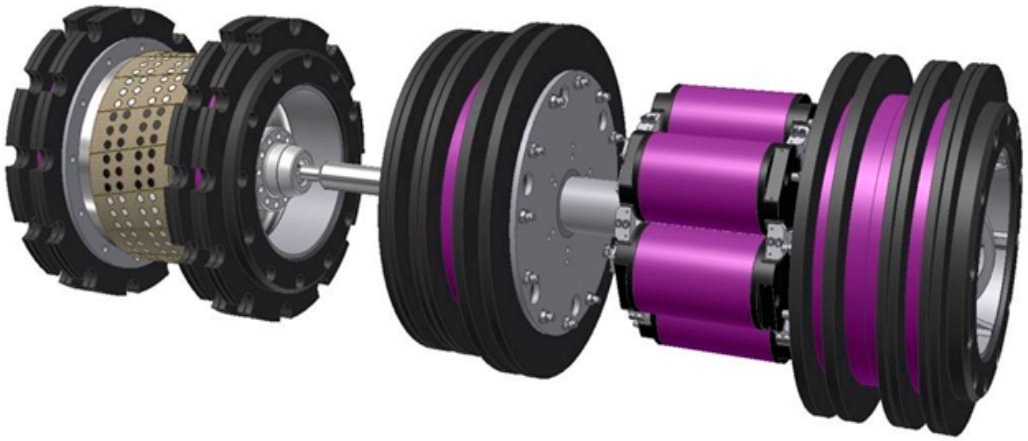

Figure 14: Illustration of the ART Scan pig. The purple front unit has discs that seal off the gas pipe and create a pressure difference, which pushes the pig forward. The rear of the unit contains the electronics and the acoustical transducers. The 192 transducers can be seen as black and white circles in this illustration.

in the tail of the signal to compute the plate thickness. It must be noted that alternative methods exist to measure plate thickness using ultrasound. The conventional ultrasound method for measuring thickness is by measuring the time-of-flight within the plate of a pulse, short enough for deconvoluting individual pulses. This means that a higher frequency needs to be used compared with the ART, or other resonance-based techniques, and a higher frequency causes increased loss. Holland and Chimenti [45] use the S_1-ZGV mode to transmit energy through a plate. They use a short, focused, broadband pulse with energy in the frequency range covering the S_1-ZGV mode. The transmitter and receiver are moved over the plate to make a C-scan image at the frequency near the S_1-ZGV mode. They show that this technique can be used for imaging thin tapes on a plate. This technique could have been used to measure thickness in a laboratory setting. However, automatic processing in practice requires more resonances to cover a range of thicknesses.

2.4 Results achieved in this thesis

This thesis presents a method to use resonances to measure the thickness of steel plates in air, using air-coupled ultrasound with through-transmission. For steel plates of thick-

ness around 10 mm, the method was able to distinguish between absolute thickness differences of 0.15 mm, or 1.5 % relative. The main sources of uncertainty in the thickness estimates were the uncertainty of the compressional and shear wave velocities in the steel plate. Alternatively, if the thickness is known, the compressional and shear wave velocities can be found. A theoretical model using the angular spectrum method was implemented and used to model the wave propagation, both in the air and the plate. The theoretical spectra calculated form this model were found to predict the resonances from the S_1, A_2, and A_3 modes, within 1 % of the measured values. These were the modes within the frequency range covered by the experiments. Compared with the simple model for plane wave, half-wavelength resonances, the frequency of the S_1 mode was observed to be shifted down by approximately 7 %.

Placing the receiver off the acoustic axis of the transmitting transducer was studied as a method to suppress the strong first signal in pulse-echo measurements. The angular spectrum method model described above was extended to cover a point receiver placed off the acoustic axis of the transmitter, for both pulse-echo and through-transmission setups. Results from this model were compared with measurements in a water tank, after transmission through a steel plate, using a hydrophone as receiver. The hydrophone could be moved laterally, and measurements were taken at different lateral displacements, compared with the acoustic axis of the transmitter. The theoretical results were found to match well with the measurements for a receiver at zero displacement, i.e. placed on the acoustic axis of the transmitter. For a laterally displaced receiver, deviations were found between the measured and theoretical results. However, the general trend in the measured results was well captured by the theoretical model.

The theoretical model was used to predict the received signals from a pulse-echo measurement on a steel plate in air. The simulation studies indicate that the first reflection energy decreases more rapidly with lateral displacement than the tail energy does. These indications are based on the predictions from our model, and not verified by measurements. If this holds, it can provide a solution to the main problem when applying the resonance method in an air-coupled pulse-echo setup: The first reflection is so strong that it will mask the later arriving parts of the signal, containing the thickness information. A laterally displaced receiver can reduce the level of the first reflection compared with the level in the tail of the signal to overcome this.

It is concluded that lateral displacement of the receiver can reduce the strong specular reflection from the air-steel interface, and hence, provide a method to make it feasible to use single-sided pulse-echo measurements to detect plate resonances and measure the thickness in steel and other materials in air. It was further found that the positions of the resonances were not sensitive to the displacement of the receiver, and the relations between the resonance peak frequencies and the plate thickness is the same as for a

receiver placed on the axis. However, some care must be taken when selecting the time window for computing the spectra, to avoid a split in the resonance peaks for certain time windows. An improved model for the transducer would have been beneficial, for instance, one based on measurements of the actual beam pattern. This might have given more accurate results at the larger displacements. Details of the transducer were not available. Furthermore, reflection measurements would have been beneficial for testing the model, but were not feasible with the equipment available.

In the simplest case of a plane wave at normal incidence, the resonance frequencies are given by the half-wavelength thickness resonances in the plate, following the well-known relation $f_n = nc_P/(2d)$. However, this model is insufficient to describe the resonance peaks occurring from a spatially bounded beam generated by a finite aperture transducer. In this thesis, the angular spectrum method was used to investigate the lowest resonance peak in spectra received after acoustic transmission through an elastic plate. *Paper C* examines how this peak deviates from the simple plane-wave model and how the peak depends on parameters of the measurement arrangement and on properties of the elastic plate.

The models assume a plane piston type vibration of the transducer surface, and use elastic wave propagation to find the transmission coefficient of the plate. It was found that the first peak in the received spectrum could be down shifted up to 11 % compared with the half wavelength compressional resonance at normal incidence, i.e. the plate cut-off frequency of the S_1-mode. The down-shift of 11 % is due to the combined effect of two sources: First, for a ratio between the compressional and shear wave velocities in the plate $\kappa > 2$, the S_1- and S_2-modes swap position, and the lower cut-off frequency of the S_2-mode is the main source of the peak. Second, since the peaks are caused by a ZGV mode, the curvature of the mode can create a down-shift, depending on the angular spectrum of the transducers and the transmission coefficient of the plate.

The down-shift of the resonance peak was found to be negligible when the opening angles of the transmitter and receiver are small compared with the critical angle, and when the distances between the plate and transducers are large compared with the Rayleigh distance. However, for large opening angles and at short distances, the angular spectrum of the sound field will excite leaky Lamb-modes at larger angles close to the ZGV mode, causing a shift in frequency compared with the plate cut-off frequency. The lowest possible value of the received resonance peak is limited by the minimum frequency of the S_1 or S_2-modes, and depends on the ratio between the compressional and shear wave velocities in the plate, $\kappa = c_p/c_s$. The upper bound for the resonance peak for materials with $\kappa < 2$, is the cut-off frequency of the S_1-mode, while for materials with $\kappa > 2$, it is the cut-off frequency of the S_2-mode. For a specific measurement setup, the actual value of the resonance peak will be found between these two limits. Looking at

other modes, there was no upward shift in the A_2-mode, despite it having a strong right bending curvature in the transmission coefficient.

The down-shift studied for through-transmission measurements, is closely related to the correction factor previously established for the Impact Echo method. The down-shift also depends on the ratio between the compressional and shear speed of sound. Analogue to the correction factor in the Impact Echo method, the study presented in this paper can be used as the basis for a correction factor for through-transmission measurements using the resonances to extract information on the plate. These results of the studies may also prove helpful when designing acoustic systems to measure thickness in plates, e.g. for selection and placement of the transducers and correction of the plane wave assumption.

Paper C contains a systematic modeling of the whole parameter space of the setup in Figure 9. Only a few of the points in the parameter space are compared with laboratory measurements, i.e. the measurements in *Paper A* and *Paper B*. More experiments with different transducer geometries, solid materials and distance from transducer to plate, could be done to corroborate this contribution.

The angular spectrum model documented in *Paper D*, was tested against measurements in a water tank. The predictions for lateral displacement of the receiver have not been tested against laboratory measurement in air. The physical process is the same in both air and water measurements. With the available equipment, i.e. transducer and electronics, it was not possible to obtain signals of sufficient quality in air, while the measurements in water give a much better signal-to-noise ratio. Measurements in air could have substantiated the conclusions, and should be possible with more optimized transducers and electronics.

The challenge with air-coupled ultrasound measurements on solids in general, and steel in particular, is the very low ratio between the characteristic acoustic impedances of air and steel, and a big difference in sound speed, resulting in a low critical angle. For a water-steel interface, these values are much more favorable. The low critical angle at the air-steel interface, less than 5°, makes the measurements susceptible to misalignment between the transducer and the steel plate. The geometry of the misalignment problem is depicted in Figure 15 and the amplitude of the reflection as a function of angle is plotted in Figure 16. In a practical setting, this is going to be a challenge since a small misalignment angle might cause the total loss of the tail signal. One possible solution is to use arrays and beamforming to compensate for the misalignment.

The low impedance ratio means that only a very small fraction of the sound energy will propagate through the air-steel interface. This makes the tail of the received signal coming from reflections inside the steel tiny, compared with the reflection from the steel

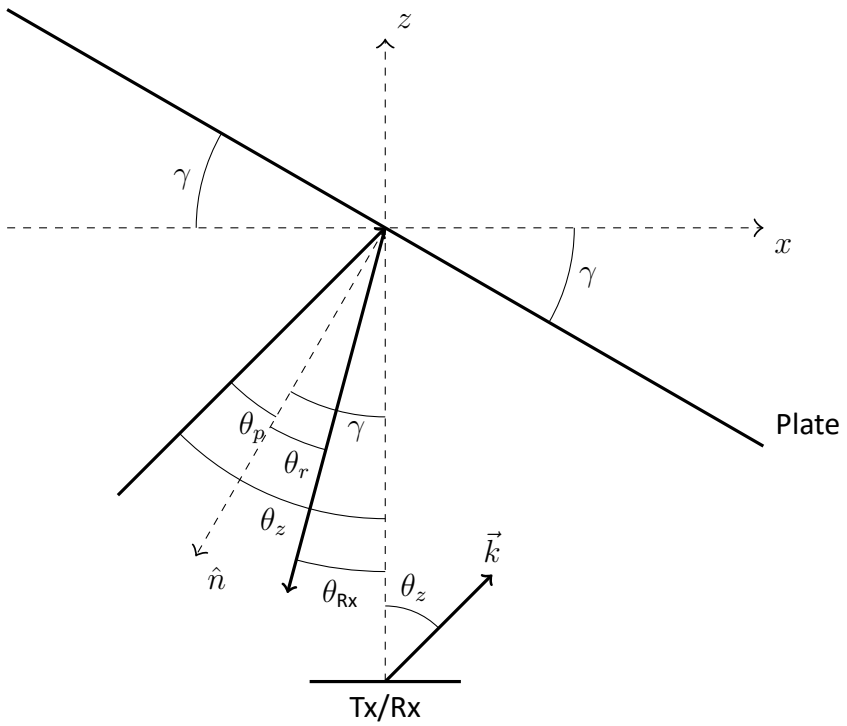

Figure 15: Illustration of the misaligned plate problem, where the misalignment angle is γ with respect to the x-axis. A wave propagates from the transmitter *Tx* at with a wavenumber $\vec{k}$ and at an angle θ_z with respect to the z-axis. $\vec{n}$ is a unit vector, normal to the plate surface. θ_p is the angle of incidence of the plane wave on the plate, and θ_r is the angle of the reflected wave.

surface. This vast difference in level is a challenge for the transducer, as the ring-down of the first reflection will have much larger amplitude than the tail signal. A large bandwidth transducer with a short ring-down time would be a benefit for this type of thickness measurement.

The conclusion for the thesis as an entity is that it is possible to measure the thickness of steel in air by using a through-transmission setup. A pulse-echo setup is more practical, but hampered by the big reflection from the air-steel interface. It is therefore proposed to move the receiver laterally away from the transmitter. Theoretical results are presented, showing that this will reduce the first reflection more than the energy in the tail, while the techniques for thickness measurements described above will still be valid. The simple plane wave, normal incidence assumption is not sufficient to describe the relation between thickness and resonance frequencies, especially for the peak associated with the first compressional resonance. A systematic study is performed on how this deviation depends on the properties of the plate and the parameters of the setup, and show how this can be resolved by either selecting a parameter region where the effect can be neglected or compensating for the effect by a correction factor.

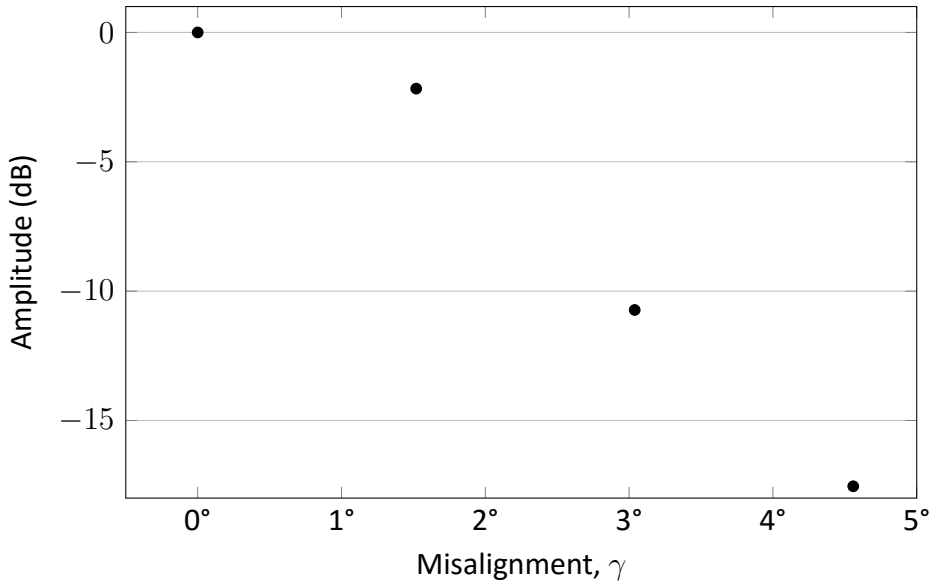

Figure 16: The amplitude of the reflection in air for different misalignment angles γ.

Chapter 3

Summary of Thesis

This thesis consists of one paper published in a peer-reviewed journal *Paper A*, one paper submitted to a peer-reviewed journal *Paper C*, one paper being an extended version of a published conference proceedings *Paper B*, and finally, a paper written as a technical manual *Paper D*. These four contributions are summarised in this section.

Paper A: Air-coupled ultrasonic through-transmission measurements of steel plates

This paper presents a laboratory experiment for ultrasonic, through-transmission measurements of a steel plate in air. The experiments were performed with a transmitter originally made for gas at high pressure, i.e. the prototype version of the ART Scan tool. The receiver was a transducer made specifically for use in air. The plate was nominally 10.15 mm thick, with two areas machined down to 10.0 mm and 9.8 mm.

The experiments showed that the three different thicknesses of the plate could be distinguished in the spectrogram of the measurement in each region. Specifically, the S_1, S_2 and A_3-modes were excited in the plate in each of the three regions. The resonance in the region of the S_1 mode was observed to be shifted down 10 % compared with the half wavelength resonance, $f_1 = \frac{c_p}{2d}$. This down-shift was further investigated in *Paper C*.

An analytical model was developed to elaborate on the forgoing observations. The model was based on the angular spectrum and included the effects of the finite apertures of the receiver, transmitter, compressional and shear waves in the steel plate. The model predicted the resonance frequencies of the plate to within 1 %, and explained the down-shift of the first compressional resonance.

This paper has been published in Ultrasonics, vol. 56, 2015 [62].

Paper B: Feasibility of pulse-echo thickness measurements in air with a laterally displaced receiver

In this paper the model developed in *Paper A* is developed to include a point receiver displaced laterally away from the acoustical axis. The model is compared against measurements in a water tank, both in the time and frequency domain, at the resonance frequencies. Petter Norli performed the measurements in the water tank at the Acoustic Resonance Technology laboratory at DNV (Det Norske Verisat). Although deviations are observed between the measurements, the model is deemed to be accurate enough to be useful for predictions.

This model is used to predict the reflection from a steel plate in air, using a laterally displaced point receiver. Specifically, the energy of the first reflection from the plate is compared with the energy of the tail, i.e. the energy reflected back and forth inside the plate, for a range of receiver displacements. The predictions show that when the receiver is displaced laterally off the acoustic axis of the transmitter, the energy in the first reflection decreases more rapidly than the energy in the tail. In addition, the sensitivity to the selection of time window for the frequency estimation of the received signal is studied. It was found that the higher order modes are robust with regard to the selection of the analysis time window, while the first resonance depends on the position of the time window, but not the down-shift of this resonance.

This paper is an extended version of a paper published in the IEEE International Ultrasonics Symposium Proceedings 2014, pp. 1029-1032 [73]. The full version is being prepared for publication in a journal.

The results of this paper are the basis of a patent application, G. Waag, P. Norli, and L. Hoff, "Pitch-catch measurements in air using acoustics," Norwegian Patent Application 20141066.

Paper C: Finite transducer aperture influence on spectra received after transmission through an elastic plate, at frequencies near the leaky S_1 and S_2 modes

A down-shift of the first resonance compared with the cut-off frequency of the S_1-mode is observed in *Paper A* and *Paper B*. The down-shift is also known from applications DNV and Halfwave have developed, e.g. the BIT (Breivoll Inspection Technologies) pipe scanner [74], but is only handled empirically for one specific setup. The down-shift is also known from the Impact echo inspection method for testing of concrete and masonry. In *Paper A*, for certain parameter combinations, we found the first compressional reso-

nance to be as low as 0.89 times the plate cut-off frequency, i.e. the simple plane wave assumption can result in errors of up to 11 % compared with the cut-off frequency of the S1-mode when estimating the plate resonance.

The down-shift was observed to be about 11 % with respect to the cut-off frequency, which limits the precision of, for instance, thickness measurements. Previous measurement taken at DNV showed a down-shift of only 6 %. This indicated that the down-shift is dependent on the measurement parameters.

In this paper, the down-shift is studied theoretically for a through-transmission measurement setup with a transmitter - elastic plate - receiver setup, by using the model documented in *Paper D*. The down-shift originates from the curvature of the S_1 or S_2-mode of the elastic plate in combination with the finite aperture of the transmitter and receiver. The problem depends on eight physical parameters that are reduced to five dimensionless parameters: the ratio of the transducer opening angle to the critical angle ratio, the ratio of the distance from transducer to plate to the Rayleigh distance ratio, the ratio κ between the compressional and shear wave velocities in the plate, the ratio of the resonance frequency to the cut-off frequency, and the fluid-solid impedance ratio. The only assumption is that the last of these is small, i.e., the characteristic acoustic impedance of the fluid is much smaller than that of the solid plate. In this case, the frequencies of the modes are mostly unaffected by the fluid. The resonance frequency to cut-off frequency ratio was then studied as a function of the remaining four parameters.

The down-shift of the first resonance compared with the cut-off frequency of the S_1-mode is found to vary between zero and 11 % for the different parameters studied. Specifically, for narrow beams, defined as when the ratios of the transducer opening angle to the critical angle of the compressional wave in the solid is below 0.1, the influence of Lamb waves in the plate can be neglected for some materials. For ratios above 0.1 the deviation can be as much as 11 %, for some of the materials studied, i.e. aluminium and copper.

The results for aluminium and copper show that these materials are special cases. Since κ for these materials is greater than two, corresponding to a Poisson's ratio greater than $1/3$, the S_2-mode causes the lowest resonance frequency for these materials, not the S_1-mode as for the other materials. S_2 is a shear mode with a lower cut-off frequency than S_1.

This paper was submitted to NDT & International in February 2017.

Paper D: Angular Spectrum Method implementation in MATLAB®

This paper is a technical user manual describing the angular spectrum method applied to the systems studied in this thesis, and how it has been implemented in MATLAB®. Using

the 2D spatial Fourier Transform the normal velocity to pressure transfer function for a transmitter - interface/medium - receiver, can be derived as an integral. The power of the Fourier Acoustics lies in the fact that once the angular spectrum is known in a plane, the pressure or velocity field can be found by phase shifting the spectrum to a new parallel plane, and then performing the inverse transform. This can be done analytically for some geometries, which are derived in this paper. The angular spectrum can be interpreted as a decomposition of the pressure field into plane waves at a range of propagation angles. This means that the effects of transmission through a plate can be incorporated directly by the plane wave transmission coefficient.

The reason for choosing the angular spectrum method over other methods, e.g. finite element models, is that the propagation of the pressure field is applied with a simple phase shift. Due to the small wavelengths in air, other methods require a large number of nodes to model the wave propagation accurately without causing numerical noise. This either limits the distance the waves can be propagated in air or requires excessive computation time.

The paper describes the installation and usage of the software and some of the details regarding computation of the transfer function for a steel plate embedded in air. In addition, it includes the derivation of the equations that are solved numerically by the software.

This paper has been prepared as a technical report, as documentation of the work performed and to make the models.

Chapter 4

Contributions

4.1 List of Contributions

Papers in international peer-reviewed journals

1. **G. Waag**, L. Hoff, and P. Norli, ”Air-coupled ultrasonic through-transmission thickness measurements of steel plates,” Ultrasonics 56 (2015) 332-339. doi:10.1016/j.ultras.2014.08.021 [62].

Papers submitted to international peer-reviewed journals

1. **G. Waag**, and L. Hoff, ”Finite transducer aperture influence on spectra received after transmission through an elastic plate, at frequencies near the leaky S_1 and S_2 modes,” manuscript submitted to *NDT & E International*, February 2017.

Published proceedings from international conferences

1. **G. Waag**, P. Norli, and L. Hoff, ”Feasibility of pulse-echo thickness measurements in air with a laterally displaced receiver,” in *IEEE Int. Ultrason. Symp.*, Chicago, Illinois, USA, 3 - 6 September 2014 [73].

2. **G. Waag**, L. Hoff, and P. Norli, ”Model for thickness measurements of steel plates using half-wave resonances,” in *IEEE Int. Ultrason. Symp. Proc.*, Dresden, Germany, 7 - 10 October 2012 [75] .

3. **G. Waag**, L. Hoff, and P. Norli, ”Air-coupled thickness measurements of steel plates,” in *IEEE Int. Ultrason. Symp. Proc*, Orlando, Florida, USA, 18 - 21 October 2011 [76].

Presentations at international conferences

1. **G. Waag**, P. Norli, and L. Hoff, Presentation, ”Feasibility of pulse-echo thickness measurements in air with a laterally displaced receiver,” in *IEEE Int. Ultrason. Symp.*, Chicago, Illinois, USA, 3 - 6 September 2014 [73].

2. **G. Waag**, L. Hoff, and P. Norli, Poster presentation, "Model for thickness measurements of steel plates using half-wave resonances," in *IEEE Int. Ultrason. Symp. Proc.*, Dresden, Germany, 7 - 10 October 2012 [75] .

3. **G. Waag**, L. Hoff, and P. Norli, Poster presentation, "Air-coupled thickness measurements of steel plates," in *IEEE Int. Ultrason. Symp. Proc*, Orlando, Florida, USA, 18 - 21 October 2011 [76].

Presentations at national conferences

1. **Grunde Waag**, and Lars Hoff, "Through transmission measurements with off axis receiver," presentation at *37th Scandinavian Symposium of Physical Acoustics*, Geilo, Norway, 2 – 5 February 2014.

2. **Grunde Waag**, and Lars Hoff, "Through-transmission thickness measurements of a steel plate in air," presentation at *36th Scandinavian Symposium of Physical Acoustics*, Geilo, Norway, 3 - 6 February 2013.

3. **Grunde Waag**, and Lars Hoff, "Acoustic Resonance Technology and thickness measurements," presentation at *34th Scandinavian Symposium of Physical Acoustics*, Geilo, Norway, 30 January - 2 February 2011.

Patent application

1. **Grunde Waag**, Petter Norli, and Lars Hoff, "Pitch-catch measurements in air using acoustics," *Patent Application 20141066, Norway*, 2014.

4.2 Corrections and comments to Paper A

After the publication of *Paper A*, we have been made aware of typographical errors and formulations that are erroneous or may be misunderstood. This is unfortunate, and this chapter has been included to correct and clarify this.

Typographical erros in Eq. (1) and Eq. (3)

In Eq. (1), a factor 2π is missing and the factor exp$(-ik_r r)$ should be removed. The correct version of Eq. (1) is

$$U(k_r, z = 0; \omega) = 2\pi \int_0^\infty u_0 J_0(k_r r) r dr \, . \tag{23}$$

As a consequence of this, the expression for $U(k_r, z = 0, \omega)$ in the following paragraph is also missing a factor 2π, and should read $U(k_r, z = 0, \omega) = \pi a^2 2\mathrm{J}_1(k_r a)/k_r a$.

The upper integration limit in Eq. (3) is $\pi/2$.The correct version of Eq. (3) should read

$$V(\omega) = 2\pi \int_0^{\pi/2} T(\omega,\theta)\frac{\cos\theta}{\rho_f c_f} k \sin\theta S(\theta, a_{\mathsf{Tx}}) S(\theta, a_{\mathsf{Rx}}) \exp\left[ik2(d_{Rx}+d_{Tx})\cos\theta\right] k\cos\theta d\theta. \tag{24}$$

This is identical to Eq. (29) in Orofino and Pedersen [58] when $a_{\mathsf{Tx}} = a_{\mathsf{Rx}} = a$, with the exception of the factor a^2 in the expression for $S(\theta, a)$ which is included to account for the radius of the transmitter and receiver. Orofino and Pedersen [58] states that the expression for the angular spectrum is proportional to the Jinc function, hence, a comparison of the scaling factors is not possible. A time harmonic factor of $\exp(-i\omega t)$ has been used.

$T(\omega,\theta)$ is the plane wave pressure transmission coefficient of the plate.

In the last paragraph of chapter 2.1.1, on page 334, the expression $\exp(-ik_z d)$ should be corrected to $\exp(ik_z d)$.

The errors stated here are typos in the text. Calculations were done using the correct values, and the results and conclusions are not influenced.

Description of $V(\omega)$

The definition of the integral in Eq. (3) in the paper (Eq. (24) above) is inaccurate. $V(\omega)$ is the transfer function from pressure at the transmitter, normalized to the transmitter area, to average normal velocity over the receiver surface. This means that the angular spectrum given in Eq. (1) and Eq. (2) represents the angular pressure spectrum, not the angular velocity spectrum as written in the text. Further details can be found in *Paper D*.

As a consequence of this, the description and notation of the transfer functions in Eq. (4), Eq. (5), Eq. (6) and Eq. (7) should be updated, by replacing some of the subscripts v with p.

The corrected transfer functions and their descriptions are now:

Eq. (4):

$$H_{\mathsf{sys}} = H_{pp}^{Tx} H_{\mathsf{plate}} H_{pv}^{Rx} \tag{25}$$

representing the transfer function from transmitter pressure to normal velocity integrated over the receiver surface. H_{pp}^{Tx} is the transfer function from pressure at the transducer surface to the pressure on the top of the plate, H_{pv}^{Rx} is the transfer function from pressure at the rear side of the plate to the normal velocity integrated over the receiver surface and H_{plate} is the transfer function from pressure at the top of the plate to the pressure at the bottom of the plate.

The equation in the last paragraph of section 2.1.1:

$$H_{\text{direct}} = H_{pp}^{Tx} H_{\text{air}} H_{pv}^{Rx} \text{.,} \tag{26}$$

Eq. (6):

$$\hat{H}_{\text{sys}} = H_{Vp}^{Tx} H_{pp}^{Tx} H_{\text{plate}} H_{pv}^{Rx} H_{vV}^{Rx}. \tag{27}$$

Eq. (7):

$$\hat{H}_{\text{direct}} = H_{Vp}^{Tx} H_{pp}^{Tx} H_{air} H_{pv} H_{vV}^{Rx}, \tag{28}$$

where H_{Vp}^{Tx} is the voltage to pressure transfer function for the transmitter and H_{vV}^{Rx} is the integrated normal velocity to voltage on the receiver.

The equation in the first paragraph of section 2.2.2:

$$H_{Vv}^{\text{Tx}-\text{Rx}} = H_{Vp}^{Tx} H_{vV}^{Rx} \text{ .} \tag{29}$$

These altered definitions of the transfer functions and the corresponding changes in notation have no influence on the results or conclusions.

Typographical error in the caption of Fig. 5

In the caption of Fig. 5, the correct plate thickness is 10 mm, not the stated 4 mm.

Some imprecise or incomplete statements

Since the handling of evanescent waves was not commented on the paper, the assumptions and approximations regarding this should be specified, as follows:
Evanescent waves are included in the plate through the transmission coefficient $T(f, \theta)$. Evanescent waves in the fluid are neglected, expressed by setting the upper integration limit in Eq. (3) to $\pi/2$. This choice is further discussed in *Paper D*.

The comment regarding the down-shift in the last paragraph of 3.3, on page 337: *"The first peak, interpreted as the half-wave pressure wave resonance or* S_1*, is found at* $f_1 \approx 0.9$*, i.e. 10% lower than predicted by the simple plane wave model. This is in accordance with the reduction in frequency with the angle shown in Fig. 3, and can be explained by the angular spread of the sound field from the transducers."*
This should be reformulated to: *"The first peak is found at* $f_1 \approx 0.9$*, i.e. 10% lower than predicted by the simple plane wave model Eq. (8). The down-shift of this resonance is previously known [45] and is related to the angular spread of the sound field from the transducers and the presence of the* S_1*-ZGV mode."*

The down-shift of the S_1-mode is a main topic of *Paper C*, and is commented further here.

In the first paragraph of Section 3.4: *"However the difference in frequency between the theoretical model and the measured spectra for the* S_1, A_2 *and* A_3*, is within 1%,"* should be corrected to: *"However the difference in the frequency of the observed peaks between the theoretical model and the measured spectra for the* S_1, A_2 *and* A_3 *modes, is within 1%."*

In Section 3.4, below Fig. 7: *"The frequency shift of the first peak (*S_1*) is most likely coming from the curvature of the transmission coefficient shown in Fig. 3, but also because it is in the transition region of the transducer's lower frequency band."* Since the down-shift of the first peak is already commented above, this sentence is just a repetition and should be removed.

The second sentence in Section 3.2: *"The resulting power spectrum is shown in Fig. 4,"* should be corrected to: *"The absolute value of the pressure to velocity transfer function is shown in Fig. 4."*

Bibliography

[1] B. Raj, T. Jayakumar, M. Thavasimuthu, Practical Non-destructive Testing, Woodhead Publishing, Cambridge, 2002, p. 1, ISBN: 9781855736009.

[2] Watching the rot, *The Economist* (2011), URL: http://www.economist.com/blogs/babbage/2011/10/corrosion-monitoring (visited on 08/31/2016).

[3] B. Raj, T. Jayakumar, M. Thavasimuthu, Practical Non-destructive Testing, Woodhead Publishing, Cambridge, 2002, ISBN: 978-1-85573-600-9.

[4] B. Raj, T. Jayakumar, M. Thavasimuthu, Practical Non-destructive Testing, Woodhead Publishing, Cambridge, 2002, pp. 4–8, ISBN: 978-1-85573-600-9.

[5] B. Raj, T. Jayakumar, M. Thavasimuthu, Practical Non-destructive Testing, Woodhead Publishing, Cambridge, 2002, pp. 8–17, ISBN: 978-1-85573-600-9.

[6] B. Raj, T. Jayakumar, M. Thavasimuthu, Practical Non-destructive Testing, Woodhead Publishing, Cambridge, 2002, pp. 17–27, ISBN: 978-1-85573-600-9.

[7] B. Raj, T. Jayakumar, M. Thavasimuthu, Practical Non-destructive Testing, Woodhead Publishing, Cambridge, 2002, pp. 54–77, ISBN: 978-1-85573-600-9.

[8] J. Blitz, Electrical and Magnetic Methods of Non-destructive Testing, Springer Science & Business Media, 2012, pp. 43–48, ISBN: 978-94-011-5818-3.

[9] J. L. Rose, Ultrasonic Guided Waves in Solid Media, Cambridge University Press, New York, 2014, p. 245, ISBN: 978-1-107-04895-9.

[10] Z. Su, L. Ye, Identification of damage using Lamb waves: from fundamentals to applications, vol. 48, Springer Science & Business Media, Berlin, 2009, pp. 186–193.

[11] J. L. Rose, Ultrasonic Waves in Solid Media, Cambridge University Press, New York, 2004, pp. 101–107, ISBN: 0-521-54889-6.

[12] D. Chimenti, Review of air-coupled ultrasonic materials characterization, *Ultrasonics* 54 (7) (2014) 1804–1816, DOI: 10.1016/j.ultras.2014.02.006.

[13] M. C. Remillieux, B. E. Anderson, T. J. Ulrich, P.-Y. Le Bas, M. R. Haberman, J. Zhu, Review of Air-Coupled Transduction for Nondestructive Testing and Evaluation, *Acoust. Today* 11 (3) (2014) 36–45.

[14] R. E. Green, Non-contact ultrasonic techniques, *Ultrasonics* 42 (1-9) (2004) 9–16, DOI: 10.1016/j.ultras.2004.01.101.

[15] D. Sancho-Knapik, H. Calas, J. J. Peguero-Pina, A. Ramos Fernandez, E. Gil-Pelegrin, T. E. Gomez Alvarez-Arenas, Air-coupled ultrasonic resonant spectroscopy for the study of the relationship between plant leaves' elasticity and their water content, *IEEE Trans. Ultrason. Ferroelectr. Freq. Control* 59 (2) (2012) 319–325, DOI: 10.1109/TUFFC.2012.2194.

[16] A. Siddiolo, L. D'Acquisto, A. Maeva, R. Maev, Wooden panel paintings investigation: An air-coupled ultrasonic imaging approach, *IEEE Trans. Ultrason. Ferroelectr. Freq. Control* 54 (4) (2007) 836–846, DOI: 10.1109/TUFFC.2007.317.

[17] M. Castaings, B. Hosten, The use of electrostatic, ultrasonic, air-coupled transducers to generate and receive Lamb waves in anisotropic, viscoelastic plates, *Ultrasonics* 36 (1-5) (1998) 361–365, DOI: 10.1016/S0041-624X(97)00144-3.

[18] J. D. Stephens, B. R. Kowalczyk, B. C. Hancock, G. Kaul, I. Akseli, C. Cetinkaya, In-die ultrasonic and off-line air-coupled monitoring and characterization techniques for drug tablets, in: vol. 1430, 1, Burlington, VT, USA, 17 - 22 July, 2011, pp. 1691–1698, DOI: doi:10.1063/1.4716416.

[19] J. Liu, N. F. Declercq, Air-coupled ultrasonic investigation of stacked cylindrical rods, *J. Acoust. Soc. Am.* 131 (6) (2012) 4500–4507, DOI: 10.1121/1.4707442.

[20] H. Tat, G. Georgeson, R. Bossi, Evaluation of air coupled ultrasound for composite aerospace structure, *AIP Conf. Proc.* 1096 (1) (22-25 July, 2008) 912–919, DOI: 10.1063/1.3114355.

[21] J. Ealo, J. Camacho, F. Seco, C. Fritsch, Ultrasonic air-coupled inspection of textile materials using ferroelectret-based phased arrays, in: vol. 1211, 1, Kingston, USA, 26–31 July 2009, pp. 933–940, DOI: 10.1063/1.3362529.

[22] D. K. Hsu, Nondestructive testing using air-borne ultrasound, *Ultrasonics* 44 (Supplement 1) (2006) e1019–e1024, DOI: 10.1016/j.ultras.2006.05.091.

[23] M. Rheinfurth, F. Schmidt, D. Doring, I. Solodov, G. Busse, P. Horst, Air-coupled guided waves combined with thermography for monitoring fatigue in biaxially loaded composite tubes, *Compos. Sci. Technol.* 71 (5) (2011) 600–608, DOI: 10.1016/j.compscitech.2010.12.012.

[24] M. Castaings, P. Cawley, R. Farlow, G. Hayward, Single sided inspection of composite materials using air coupled ultrasound, *J. Nondestruct. Eval.* 17 (1) (1998) 37–45.

[25] F. Siegmund, D. Döring, M. Rheinfurth, E. Haberstroh, G. Busse, Air-coupled Ultrasound for Monitoring the Production of PUR Sandwich Structures, *Int. Polym. Proc.* XXV (05) (2010) 372–378, DOI: 10.3139/217.2358.

[26] D. A. Soto, R. A. Salas, T. E. G. Alvarez-Arenas, Air-coupled ultrasonic spectroscopy applied to the study of the properties of paper produced from mineral powder (mineral paper), in: vol. 1433, 1, Gdańsk, Poland, 5–8 September 2011, pp. 155–158, DOI: 10.1063/1.3703160.

[27] T. Gomez, B. Gonzalez, F. Montero, Paper characterization by measurement of thickness and plate resonances using air-coupled ultrasound, in: IEEE Int. Ultrason. Symp. Proc., vol. 1, Munich, Germany, 8 - 11 October,2002, 865–868 vol.1, ISBN: 1051-0117, DOI: 10.1109/ULTSYM.2002.1193534.

[28] T. Alvarez-Arenas, J. Benedito, E. Corona, Non-contact ultrasonic assessment of the properties of vacuum-packaged dry-cured ham, in: IEEE Ultrason. Symp. Proc., Rome, Italy, 20 - 23 Sept. 2009, pp. 2541–2544, ISBN: 1948-5719, DOI: 10.1109/ULTSYM.2009.5441742.

[29] P. Pallav, D. Hutchins, T. Gan, Air-coupled ultrasonic evaluation of food materials, *Ultrasonics* 49 (2) (2009) 244–253, DOI: 10.1016/j.ultras.2008.09.002.

[30] S. Delrue, K. Van Den Abeele, E. Blomme, J. Deveugele, P. Lust, O. B. Matar, Two-dimensional simulation of the single-sided air-coupled ultrasonic pitch-catch technique for non-destructive testing, *Ultrasonics* 50 (2) (2010) 188–196, DOI: 10.1016/j.ultras.2009.08.005.

[31] D. W. Schindel, D. S. Forsyth, D. A. Hutchins, A. Fahr, Air-coupled ultrasonic NDE of bonded aluminum lap joints, *Ultrasonics* 35 (1) (1997) 1–6, DOI: 10.1016/S0041-624X(96)00088-1.

[32] T. J. Potter, B. Ghaffari, G. Mozurkewich, Sub-wavelength resolution in air-coupled ultrasound images of spot welds, *NDT&E Int.* 38 (5) (2005) 374–380, DOI: 10.1016/j.ndteint.2004.10.010.

[33] M. Castaings, P. Cawley, The generation, propagation, and detection of Lamb waves in plates using air-coupled ultrasonic transducers, *J. Acoust. Soc. Am.* 100 (5) (1996) 3070–3077, DOI: 10.1121/1.417193.

[34] W. M. D. Wright, D. A. Hutchins, Air-coupled ultrasonic testing of metals using broadband pulses in through-transmission, *Ultrasonics* 37 (1) (1999) 19–22, DOI: 10.1016/S0041-624X(98)00034-1.

[35] Y. Yanez, M. Garcia-Rodriguez, M. J. Garcia-Hernandez, J. Salazar, A. Turo, J. A. Chavez, P3F-1 Lamb Wave Generation with an Air-Coupled Piezoelectric Array Using Different Square Chirp Modulation Schemes, in: IEEE Int. Ultrason. Symp. Proc., New York, USA, 28th - 31st Oct. 2007, pp. 1844–1847, DOI: 10.1109/ULTSYM.2007.464.

[36] H. Ogi, M. Hirao, T. Honda, Ultrasonic attenuation and grain-size evaluation using electromagnetic acoustic resonance, *J. Acoust. Soc. Am.* 98 (1) (1995) 458–464, DOI: 10.1121/1.413703.

[37] W. Ke, M. Castaings, C. Bacon, 3D finite element simulations of an air-coupled ultrasonic NDT system, *NDT & E Int.* 42 (6) (2009) 524–533, DOI: 10.1016/j.ndteint.2009.03.002.

[38] H. Lamb, On Waves in an Elastic Plate, *Proc. R. Soc. Lon. Ser-A* 93 (1917) 114–128, DOI: 10.1098/rspa.1917.0008.

[39] M. Aanes, Interaction of piezoelectric transducer excited ultrasonic pulsed beams with a fluid-embedded viscoelastic plate. Finite element modeling, angular spectrum modeling and measurements, PhD thesis, University of Bergen, Department of Physics and Technology, 2014, ISBN: 978-82-308-2946-2.

[40] C. Prada, D. Clorennec, D. Royer, Local vibration of an elastic plate and zero-group velocity Lamb modes, *J. Acoust. Soc. Am.* 124 (1) (2008) 203–212, DOI: 10.1121/1.2918543.

[41] K. F. Graff, Wave Motion in Elastic Solids, Dover Publications, New York, 1991, p. 449, ISBN: 0486667456.

[42] J. Jocker, D. Smeulders, Minimization of finite beam effects in the determination of reflection and transmission coefficients of an elastic layer, *Ultrasonics* 46 (1) (2007) 42–50, DOI: 10.1016/j.ultras.2006.10.001.

[43] D. E. Chimenti, S. I. Rokhlin, Relationship between leaky Lamb modes and reflection coefficient zeroes for a fluid-coupled elastic layer, *J. Acoust. Soc. Am.* 88 (3) (1990) 1603–1611, DOI: 10.1121/1.400319.

[44] I. Tolstoy, E. Usdin, Wave Propagation in Elastic Plates: Low and High Mode Dispersion, *J. Acoust. Soc. Am.* 29 (1) (1957) 37–42, DOI: 10.1121/1.1908675.

[45] S. D. Holland, D. E. Chimenti, Air-coupled acoustic imaging with zero-group-velocity Lamb modes, *Appl. Phys. Lett.* 83 (13) (2003) 2704–2706, DOI: 10.1063/1.1613046.

[46] C. Prada, D. Clorennec, D. Royer, Power law decay of zero group velocity Lamb modes, *Wave Motion* 45 (6) (2008) 723–728, DOI: 10.1016/j.wavemoti.2007.11.005.

[47] J. Laurent, D. Royer, C. Prada, Temporal behavior of laser induced elastic plate resonances, *Wave Motion* 51 (6) (2014) 1011–1020, DOI: 10.1016/j.wavemoti.2014.04.001.

[48] S. D. Holland, S. V. Teles, D. E. Chimenti, Air-coupled, focused ultrasonic dispersion spectrum reconstruction in plates, *J. Acoust. Soc. Am.* 115 (6) (2004) 2866, DOI: 10.1121/1.1710501.

[49] F. Ahmad, T. Hussain, Anomalous Dispersion of the S1 Lamb Mode, *Adv. Acoust. Vib.* 2013 (2013) 1–6, DOI: 10.1155/2013/903934.

[50] C. B. Scruby, L. E. Drain, Laser Ultrasonics Techniques and Applications, CRC Press, New York, USA, 1990, ISBN: 978-0-7503-0050-6.

[51] C. Mattei, L. Adler, Leaky wave detection at air–solid interfaces by laser interferometry, *Ultrasonics* 38 (1–8) (2000) 570–574, DOI: dx.doi.org/10.1016/S0041-624X(99)00133-X.

[52] X. Jia, C. Matteï, G. Quentin, Analysis of optical interferometric measurements of guided acoustic waves in transparent solid media, *J. Appl. Phys.* 77 (11) (1995) 5528–5537, DOI: 10.1063/1.359592.

[53] X. Jia, G. Quentin, M. Lassoued, Optical heterodyne detection of pulsed ultrasonic pressures, *IEEE Trans. Ultrason. Ferroelectr. Freq. Control* 40 (1) (1993) 67–69, DOI: 10.1109/58.185000.

[54] D. Clorennec, C. Prada, D. Royer, Local and noncontact measurements of bulk acoustic wave velocities in thin isotropic plates and shells using zero group velocity Lamb modes, *J. Appl. Phys.* 101 (3) (2007) 034908, DOI: 10.1063/1.2434824.

[55] *Nondestructive test methods for evaluation of concrete in structures*, ACI 228.2R-98, American Concrete Institute (ACI), 1998.

[56] A. Gibson, J. S. Popovics, Lamb Wave Basis for Impact-Echo Method Analysis, *J. Eng. Mech.* 131 (4) (2005) 438–443, DOI: 10.1061/(ASCE)0733-9399(2005)131:4(438).

[57] Y.-T. Tsai, J. Zhu, Simulation and Experiments of Airborne Zero-Group-Velocity Lamb Waves in Concrete Plate, *J. Nondestruct. Eval.* 31 (4) (2012) 373–382, DOI: 10.1007/s10921-012-0148-6.

[58] D. P. Orofino, P. C. Pedersen, Evaluation of angle-dependent spectral distortion for infinite, planar elastic media via angular spectrum decomposition, *J. Acoust. Soc. Am.* 93 (3) (1993) 1235–1248.

[59] E. G. Williams, ed., Index, Academic Press, London, 1999, pp. 296–306, ISBN: 978-0-12-753960-7, DOI: http://dx.doi.org/10.1016/B978-012753960-7/50009-7.

[60] P. Cawley, B. Hosten, The use of large ultrasonic transducers to improve transmission coefficient measurements on viscoelastic anisotropic plates, *J. Acoust. Soc. Am.* 101 (3) (1997) 1373–1379.

[61] K. D. Lohne, P. Lunde, M. Vestrheim, Measurements and 3D simulations of directive beam transmission through a water-immersed steel plate, in: Proc. 34th Scand. Symp. Phys. Acoust., The Norwegian Physical Society, Geilo, Norway, 30 Jan. - 2 Feb. 2011, ISBN: 978-82-81223-004-0.

[62] G. Waag, L. Hoff, P. Norli, Air-coupled ultrasonic through-transmission thickness measurements of steel plates, *Ultrasonics* 56 (2015) 332–339, DOI: 10.1016/j.ultras.2014.08.021.

[63] M. Aanes, K. D. Lohne, E. Storheim, P. Lunde, M. Vestrheim, Beam transmission of water-embedded steel plate at normal incidence. Diffraction effects in the S1 to A3 region, in: Proc. 38th Scand. Symp. Phys. Acoust., The Norwegian Physical Society, Geilo, Norway, 1 - 4 Feb. 2015, ISBN: 978-82-8123-013-2.

[64] R. K. Johnson, A. J. Devaney, Transducer effects in acoustic scattering measurements, *Appl. Phys. Lett.* 41 (7) (1982) 622, DOI: 10.1063/1.93628.

[65] R. Demirli, J. Saniie, Model-based estimation of ultrasonic echoes. Part I: Analysis and algorithms, *IEEE Trans. Ultrason. Ferroelectr. Freq. Control* 48 (3) (2001) 787–802, DOI: 10.1109/58.920713.

[66] N. Etaix, A. Leblanc, M. Fink, Ing, Thickness or phase velocity measurements using the Green's function comparison method, *IEEE Trans. Ultrason. Ferroelectr. Freq. Control* 57 (8) (2010) 18804–1812, DOI: 10.1109/TUFFC.2010.1618.

[67] W. Gao, C. Glorieux, J. Thoen, Laser ultrasonic study of Lamb waves: determination of the thickness and velocities of a thin plate, *Int. J. Eng. Sci.* 41 (2) (2003) 219–228, DOI: 10.1016/S0020-7225(02)00150-7.

[68] D. Fei, D. E. Chimenti, S. V. Teles, Material property estimation in thin plates using focused, synthetic-aperture acoustic beams, *J. Acoust. Soc. Am.* 113 (5) (2003) 2599–2610.

[69] T. E. Gómez Álvarez-Arenas, Simultaneous determination of the ultrasound velocity and the thickness of solid plates from the analysis of thickness resonances using air-coupled ultrasound, *Ultrasonics* 50 (2) (2010) 104–109, DOI: 10.1016/j.ultras.2009.09.009.

[70] C. S. McIntyre, D. A. Hutchins, D. R. Billson, J. Stor-Pellinen, The use of air-coupled ultrasound to test paper, *IEEE Trans. Ultrason. Ferroelectr. Freq. Control* 48 (3) (2001) 717–727, DOI: 10.1109/58.920699.

[71] *Halfwave AS*, URL: http://www.halfwave.com (visited on 08/31/2016).

[72] *Breivoll Inspection Technologies AS*, URL: http://breivoll.no (visited on 08/31/2016).

[73] G. Waag, L. Hoff, P. Norli, Feasibility of pulse-echo thickness measurements in air with a laterally displaced receiver, in: IEEE Int. Ultrason. Symp. Proc., Chicago, IL, USA, 3. - 6. Sept. 2014, pp. 1029–1032, DOI: 10.1109/ULTSYM.2014.0252.

[74] M. H. Skjelvareid, Synthetic aperture ultrasound imaging with application to interior pipe inspection, PhD thesis, University of Tromsø, Department of Physics and Technology, 2012.

[75] G. Waag, L. Hoff, P. Norli, Air-coupled thickness measurements of steel plates (Poster), in: IEEE Int. Ultrason. Symp. Proc., Orlando, FL, USA, 7. - 11. Oct. 2011.

[76] G. Waag, L. Hoff, P. Norli, Air-coupled thickness measurements of stainless steel, *ArXiv e-prints* (2012).

Paper A

Air-coupled ultrasonic through-transmission thickness measurements of steel plates

Grunde Waag[a], **Lars Hoff**[b], **Petter Norli**[c]

[a] Department of Maritime Technology and Innovation, Vestfold University College, Horten, Norway

[b] Department of Micro and Nano Systems Technology, Vestfold University College, Horten, Norway

[c] Halfwave AS, Høvik, Norway

This paper is published in Ultrasonics, available online 16 September 2014 [62].

Errors identified after publication of this paper are commented in Chapter 4.2.

Paper B

Feasibility of pulse-echo thickness measurements in air with a laterally displaced receiver

Grunde Waag[a], Petter Norli[c], Lars Hoff[b],

[a] Department of Maritime Technology and Innovation, University College of Southeast Norway, Horten, Norway

[b] Department of Micro and Nano Systems Technology, University College of Southeast Norway, Horten, Norway

[c] Halfwave AS, Høvik, Norway

This paper is an extended version of a paper published in the IEEE International Ultrasonics Symposium Proceedings 2014, pp. 1029-1032, September 3-6, Chicago, IL, USA [73].

Paper omitted from
online edition due to
publisher's restrictions

Paper C

Finite transducer aperture influence on spectra received after transmission through an elastic plate, at frequencies near the leaky S_1 and S_2 modes.

Grunde Waag[a], **Lars Hoff**[b]

[a] Department of Maritime Technology and Innovation, University College of Southeast Norway, Horten, Norway

[b] Department of Micro and Nano Systems Technology, University College of Southeast Norway, Horten, Norway

This paper has been submitted to NDT & E International in February 2017.

Paper omitted from
online edition due to
publisher's restrictions

Paper D

Angular spectrum method implementation in MATLAB®

Grunde Waag[a]

[a] Department of Maritime Technology and Innovation, University College of Southeast Norway, Horten, Norway

This paper is a technical manual and not intended for publication.